GLP is critical for oogenesis exhibiting a G9A-independent role in transcriptional repression

Hannah Demond[1,2], Courtney W Hanna[1,3,4], Juan Castillo-Fernandez[1], Fátima Santos[1,3], Evangelia K Papachristou[5], Anne Segonds-Pichon[6], Kamal Kishore[5], Clive S D'Santos[5], Gavin Kelsey[1,3,7]*

[1]Epigenetics Programme, Babraham Institute, Cambridge CB22 3AT, United Kingdom

[2]Laboratory of Integrative Biology, Scientific & Technological Bioresource Nucleus Center for Excellence in Translational Medicine (BIOREN-CEMT), Universidad de la Frontera, Temuco, 4810296, Chile

[3]Centre for Trophoblast Research, University of Cambridge, Cambridge CB2 3EG, United Kingdom

[4]Department of Physiology, Development and Neuroscience, University of Cambridge, Cambridge CB2 3EG, United Kingdom

[5]Cancer Research UK Cambridge Institute, Li Ka Shing Centre, University of Cambridge, Robinson Way, Cambridge CB2 0RE, United Kingdom

[6]Bioinformatics Group, Babraham Institute, Cambridge CB22 3AT, United Kingdom

[7]Wellcome-MRC Institute of Metabolic Science-Metabolic Research Laboratories, Cambridge CB2 0QQ, United Kingdom

*Corresponding author: Gavin Kelsey (gavin.kelsey@babraham.ac.uk)

Abstract

GLP (EHMT1) functions as an H3K9me1 and H3K9me2 methyltransferase through its reportedly obligatory dimerization with G9A (EHMT2). Here, we investigated the role of GLP in oocyte and embryo development in comparison to G9A using oocyte-specific conditional knockout mouse models (*G9a* cKO, *Glp* cKO, *G9a-Glp* cDKO). Loss of GLP in oogenesis severely impairs oocyte maturation, fertilization and embryo development, resulting in lethality before embryonic day E12.5. In contrast, loss of G9A has a milder effect with a proportion of embryos producing viable offspring. The *Glp* cKO also showed loss of G9A protein and, hence, was phenotypically very similar to the *G9a-Glp* cDKO. H3K9me2 was equally depleted in all cKO genotypes, whereas H3K9me1 was decreased only in *Glp* cKO and *G9a-Glp* cDKO oocytes. Furthermore, the transcriptome, DNA methylome and proteome were markedly more affected in *G9a-Glp* cDKO than *G9a* cKO oocytes, demonstrating that in the absence of GLP there are widespread epigenetic and gene expression changes in the oocyte independent of H3K9me2. Gene dysregulation with coupled changes in DNA methylation suggest localised loss of chromatin repression, resulting in upregulated protein expression. Together, our findings demonstrate that GLP can function independently of G9A in the oocyte and is required for oocyte developmental competence.

Keywords

Oocyte, epigenetics, histone modification, histone methyltransferase, H3K9 methylation, DNA methylation, GLP/EHMT1

40 ## Introduction

41 The mammalian germline is the context for widespread epigenetic reprogramming, in which the
42 somatic epigenetic signature is erased and replaced by a germline signature that is distinct in sperm
43 and oocyte. Prior to the onset of gametogenesis, primordial germ cells undergo complete erasure of
44 epigenetic marks, such as DNA methylation (Guibert et al. 2012; Seisenberger et al. 2012) and histone-
45 3 lysine-9 dimethylation (H3K9me2) (Seki et al. 2005). In the oocyte, reprogramming occurs
46 postnatally during oocyte growth, resulting in a unique DNA methylation and histone modification
47 landscape (Hanna et al. 2018a). As the oocyte does not divide during these processes, the oocyte can
48 serve as a tractable system to study epigenetic regulation. Importantly, resetting of epigenetic marks
49 is essential to support successful oogenesis, oocyte-to-embryo transition, as well as embryonic
50 development (e.g. Kaneda et al. 2004; Andreu-Vieyra et al. 2010; Eymery et al. 2016; Kim et al. 2016;
51 Xu et al. 2019).

52 G9A (EHMT2) and GLP (EHMT1) are best known as histone methyltransferases, although they modify
53 non-histone targets as well. They preferentially function as heterodimers *in vivo* and comprise the
54 main H3K9 mono- and di-methyltransferases in euchromatin (Tachibana et al. 2001; Peters et al. 2003;
55 Rice et al. 2003; Tachibana et al. 2005; Tachibana et al. 2008). Both proteins contain a SET-domain,
56 required for their catalytic activity as methyltransferases and heterodimer formation, as well as an
57 ankyrin repeat domain that enables binding to H3K9me1 and H3K9me2 (Tachibana et al. 2001; Collins
58 et al. 2008). They have been shown to be interdependent, as H3K9me1 and H3K9me2 levels are
59 equally depleted in *G9a* KO and *Glp* KO embryonic stem cells (ESCs) (Tachibana et al. 2005). Moreover,
60 *G9a* and *Glp* KO mouse models show very similar phenotypes with embryos displaying loss of
61 H3K9me2, growth retardation and embryonic lethality between embryonic day (E)8.5 and E12.5
62 (Tachibana et al. 2002; Tachibana et al. 2005). As such, studies often do not distinguish between G9A
63 and GLP, or solely consider G9A, resulting in limited knowledge of GLP function. However, recent

64 findings indicate that GLP can act independently of G9A, revealing a role for GLP in targeting
65 H3K27me2 to the paternal pronucleus in the zygote (Meng et al. 2020).

66 In the oocyte, loss of G9A impairs maturation and meiosis, with consequences for preimplantation
67 development, leading to partial embryonic lethality (Au Yeung et al. 2019). However, some embryos
68 lacking oocyte-derived G9A develop to term and result in healthy pups. The role of GLP in the oocyte
69 and its impact on embryo development remain unclear. To investigate the importance of maternal
70 GLP in the oocyte and embryo and compare its function to G9A, we used cKO mice for *G9a* and *Glp*,
71 as well as a *G9a-Glp* cDKO. We compared the progression of oogenesis and embryogenesis in each
72 cKO, and evaluated changes in H3K9 methylation, gene expression, DNA methylation and protein
73 abundance in cKO oocytes. Our findings demonstrate that GLP has a unique and essential function in
74 the oocyte.

75

76 Results

77 GLP and G9a function during oocyte maturation and meiosis

78 To analyse the function of GLP in oocytes and compare it to that of G9A, we generated three cKO
79 models. Mice carrying floxed alleles for *G9a* (*G9a* cKO) (Sampath et al. 2007), *Glp* (*Glp* cKO) (Schaefer
80 et al. 2009) or both *G9a* and *Glp* (*G9a-Glp* cDKO) were crossed with a *Zp3*-Cre driver, which is
81 expressed exclusively in growing oocytes after postnatal day 5 (Lan et al. 2004). During oocyte
82 maturation in the ovary, the germinal vesicle (GV) oocyte undergoes a change in chromatin
83 conformation from a non-surrounded nucleolus (NSN) to a surrounded nucleolus (SN) stage that
84 coincides with global transcriptional silencing. In control animals, immunofluorescence (IF) analysis
85 showed that G9A and GLP are detected throughout the nucleus of NSN oocytes, but were no longer
86 detectable by the mature SN stage (**Supplemental Fig. S1A,B**). In *G9a* cKO oocytes, G9A protein was
87 lost in NSN oocytes, while GLP remained detectable (**Fig. 1A**). In contrast, *Glp* cKO oocytes were

88 depleted for both G9A and GLP, similar to *G9a-Glp* cDKO oocytes, indicating that GLP is required for
89 G9A stability but not *vice versa*, as was previously shown in mouse ESCs (**Fig. 1A**) (Tachibana et al.
90 2005).

91 Loss of G9A has been shown to affect oocyte maturation and meiosis (Au Yeung et al. 2019). To assess
92 whether loss of GLP has additional effects on developmental capacity of the oocyte, we first analysed
93 the NSN-to-SN maturation rate by staining fully-grown GV oocytes with DAPI and staging them
94 according to chromatin conformation. In *Glp* cKO and *G9a-Glp* cDKO oocytes from 12-week old
95 females the proportion of SN oocytes was significantly lower than in *G9a* cKO and control oocytes (**Fig.**
96 **1B**), indicating that loss of GLP has a stronger effect on oocyte maturation than loss of G9A alone.

97 To determine whether GLP is required for meiosis, we analysed spindle conformation and
98 chromosome alignment of ovulated metaphase II (MII) oocytes after hormonal stimulation. In all three
99 cKO models, an increase in abnormal chromatin configuration and spindle alignment was observed
100 compared to controls, although variation between mice was high and differences did not reach
101 statistical significance (**Fig. 1C**). Many meiotic abnormalities were observed, ranging from
102 chromosomes that were located together but not aligned ("aggregates"), chromosome alignments
103 where one or several chromosomes were misaligned, to chromosomes scattered throughout the
104 nucleus (**Supplemental Fig. S1C,D**). Spindle abnormalities included collapsed, mono- or multipolar
105 spindles (**Fig. 1C** and **Supplemental Fig. S1C**). Taken together, the results show that loss of G9A has
106 mild effects on oocyte maturation compared to the significant impairment caused by loss of GLP, while
107 effects on meiosis were similar.

108

109 **Loss of maternal GLP but not G9A results in prenatal developmental arrest**

110 To assess whether loss of GLP also compromises competence of oocytes, we examined developmental
111 progression of embryogenesis. E3.5 embryos were collected from cKO females naturally mated with

112 wildtype (WT) C57Bl/6Babr males and scored according to developmental stage. The majority of
113 embryos from control females had reached the blastocyst stage (**Fig. 1D**). In comparison, fewer
114 embryos derived from cKO oocytes progressed to blastocysts, with the proportion of maternal *G9a-*
115 *Glp* cDKO blastocysts significantly reduced, and the proportion of maternal *G9a-Glp* cDKO embryos
116 arrested at the 1-cell stage significantly increased.

117 To determine the stage of embryo arrest, embryos were collected from superovulated, naturally
118 mated cKO females at E1.5 and cultured *in vitro* for 3 days until day E4.5. Already at E1.5 a difference
119 was observed, all three cKO models having a higher proportion of unfertilized oocytes and 1-cell
120 embryos than controls. The *G9a-Glp* cDKO again showed the strongest phenotype, having significantly
121 fewer 2-cell embryos than controls (**Supplemental Fig. S2A**). Fertilized embryos (1- and 2-cell) were
122 selected for *in vitro* culture: none of the embryos from *Glp* cKO or *G9a-Glp* cDKO oocytes developed
123 to blastocysts, arresting at earlier stages (1 to 4-cell stage) by E3.5 (**Supplemental Fig. S2B,C**). In
124 contrast, 42.9% maternal *G9a* cKO embryos developed at least to morulae by E3.5 (**Supplemental Fig.**
125 **S2B,C**). However, this was significantly less than controls where 91.1% of embryos reached morula or
126 blastocyst stages by E3.5. These findings reveal that embryos derived from *G9a* cKO oocytes show
127 reduced survival through preimplantation development, whereas preimplantation developmental
128 competence of *Glp* cKO and *G9a-Glp* cDKO oocytes was severely impaired.

129 A small percentage of embryos from *Glp* cKO oocytes did progress *in vivo* to blastocysts, therefore we
130 examined the implantation and development of embryos after natural mating. In line with findings
131 above, there were significantly fewer implanted embryos at E6.5 from *Glp* cKO and *G9a-Glp* cDKO
132 oocytes than *G9a* cKO and controls (**Fig. 1E**). At E8.5, 3 maternal *Glp* cKO and 6 *G9a-Glp* cDKO embryos
133 were recovered: all were highly abnormal, with no clear tissue types or only extraembryonic tissue
134 (**Supplemental Fig. S2D,E**). In contrast, although some abnormalities (predominantly developmental
135 delay, but also abnormal morphology) were observed among E8.5 embryos from *G9a c*KO oocytes,
136 most appeared normal (**Supplemental Fig. S2D,E**). By E12.5, 55% (11/25) embryos from *G9a* cKO

137 oocytes were grossly abnormal or exhibited developmental delay (**Supplemental Fig. S2F,G**). In *G9a-*
138 *Glp* cDKO females, with one exception, all embryos had died and only resorption sites were observed
139 (**Supplemental Fig. S2F**).

140 Finally, we analysed the number of live pups born after mating cKO females with WT males: no pups
141 were born to *Glp* cKO or *G9a-Glp* cDKO females, but *G9a* cKO females did give birth to a mean of 3.46
142 healthy pups per litter, although litter size was significantly reduced compared to controls (**Fig. 1F**).
143 These results confirm previous findings in showing that although loss of G9A in the oocyte affects
144 developmental capacity of pre- and post-implantation embryos, some embryos develop normally
145 resulting in birth of healthy pups (Au Yeung et al. 2019). Our results show loss of GLP in the oocyte
146 severely impairs embryonic development and although a small proportion of embryos reach the
147 blastocyst stage and implant they die *in utero* between E8.5 and E12.5.

148

149 **Differential effects of loss of GLP or G9A on H3K9 methylation**

150 GLP and G9A are H3K9 methyltransferases required for establishment of H3K9me1 and H3K9me2 in
151 euchromatin (Tachibana et al. 2001; Tachibana et al. 2002; Tachibana et al. 2005). Therefore, we
152 examined H3K9 methylation in NSN-stage GV oocytes from cKO females (12 weeks) by IF. Consistent
153 with previous reports (Peters et al. 2003; Rice et al. 2003), H3K9me1 and H3K9me2 were localized
154 mainly in euchromatic chromatin of NSN oocytes, whereas H3K9me3 was enriched in heterochromatic
155 foci (**Fig. 2A**). Fluorescence intensity of H3K9me1 was significantly reduced in *Glp* cKO and *G9a-Glp*
156 cDKO oocytes compared to controls, but not in *G9a* cKO oocytes; in contrast, H3K9me2 decreased
157 significantly in all three cKOs (**Fig. 2A,B**). A small but significant loss of H3K9me3 was observed in *G9a-*
158 *Glp* cDKO oocytes (**Fig. 2A,B**). Rather than a direct effect, this may result from loss of H3K9me1, as the
159 H3K9me3 methyltransferase SUV39H requires H3K9me1 as a substrate (Pinheiro et al. 2012).

160 With H3K9me1 and H3K9me2 affected by loss of G9A and/or GLP, we sought to evaluate the genomic
161 localisation of these marks by ultra low-input native ChIP-seq (ULI-nChIP-seq) in WT GV oocytes from
162 15 and 25-day old females. We were able to obtain quality ChIP-seq libraries for H3K9me2 (**Fig. 2C**),
163 but not for H3K9me1. By quantifying 10kb running windows, we observed a reproducible H3K9me2
164 enrichment between replicates from d15 and d25 WT oocytes, with d25 showing greater enrichment
165 than d15 GV oocytes (**Fig. 2C, Supplemental Fig. S3A**). H3K9me2-enriched domains in d25 GV oocytes
166 were defined by merging consecutive 10kb windows with a Log_2RPKM>2.5 (34,192 or 12.5% of total
167 10kb windows; 12,514 domains; **Fig. 2C, Supplemental Fig. S3B; Supplemental Table S1**). To link
168 H3K9me2 enrichment to transcription levels, we used published data to define CpG-island (CGI) and
169 non-CGI promoters of low (FPKM<0.1), medium (FPKM 0.1-1.0) and high (FPKM>1.0) expressed genes
170 (Veselovska et al. 2015), and then compared the overlap of these promoters with H3K9me2-enriched
171 or random domains (**Supplemental Fig. S3C**). There was no difference in transcription level between
172 genes localised to H3K9me2-enriched domains or random domains, thus H3K9me2 does not appear
173 to act as a transcriptional repressor in oocytes.

174 We then assayed H3K9me2 in replicates of *G9a* cKO, *G9a-Glp* cDKO, and littermate control d25 GV
175 oocytes. Notably, H3K9me2 libraries from control oocytes were 4.94% of total chromatin, whereas
176 H3K9me2 libraries from *G9a* cKO and *G9a-Glp* cDKO oocytes were only 0.58% and 0.33%, respectively
177 (**Fig. 2D**), confirming that H3K9me2 is almost completely absent from cKO oocytes. Principal
178 component analysis (PCA) of all biological replicates showed that *G9a* cKO and *G9a-Glp* cDKO
179 H3K9me2 replicates clustered apart from control, d15 WT and d25 WT H3K9me2 replicates (**Fig. 2E**).
180 When comparing enrichment across H3K9me2-enriched domains (+/-5kb), *G9a* cKO and *G9a-Glp*
181 cDKO showed significant loss of H3K9me2 compared to controls, with enrichment comparable to that
182 in the IgG control (**Fig. 2F**). Furthermore, this effect was specific to H3K9me2-enriched domains, as
183 there was no observable difference in enrichment between cKOs and controls across a set of random
184 domains (**Fig. 2F**). There was a similar loss of H3K9me2 in *G9a* cKO and *G9a-Glp* cDKO oocytes,
185 supporting the IF results that G9A and GLP are both required for H3K9me2 in oogenesis.

186

187 **Dysregulation of proteins associated with meiosis, fertilization and oocyte function in *G9a-Glp* cDKO**
188 **oocytes**

189 Beside their role as histone methyltransferases, G9A and GLP are known to methylate non-histone
190 proteins and, by doing so, can potentially modulate their function, localisation or stability. To assess
191 whether loss of GLP affects protein abundance in the oocyte, we performed low-input (200 oocytes)
192 quantitative whole-proteome mass spectrometry isobaric labelling analysis of control, *G9a* cKO and
193 *G9a-Glp* cDKO GV oocytes. In total, 21,358 peptides were detected at FDR<1% and 3,182 quantified
194 proteins (**Supplemental Table S2**). Gene ontology (GO) analysis showed enrichment for processes
195 involved in cellular localization and organization, as well as protein folding, metabolic processes and
196 fertilization (**Fig. 3A**). Furthermore, among the top 50 most abundant proteins, we detected oocyte-
197 specific proteins such as members of the subcortical maternal complex (PADI6, NLRP5, NLRP14, TLE6,
198 KHDC3, NLRP4F), the zona pellucida (ZP1, ZP2, ZP3), as well as proteins known to be highly abundant
199 in the oocyte (DNMT1, UHRF1).

200 Comparing *G9a-Glp* cDKO with control oocytes, we identified 187 proteins with a significant change
201 in abundance (P<0.05 and Log_2FC>0.3; **Fig. 3B-D, Supplemental Table S2**). In contrast, there were only
202 38 differentially abundant proteins in *G9a* cKO oocytes, of which 21 overlapped with those in *G9a-Glp*
203 cDKO oocytes. The majority of changing proteins increased in abundance in both *G9a* cKO (12 down,
204 26 up) and *G9a-Glp* cDKO oocytes (12 down, 175 up; **Fig. 3B,C**). Although few proteins were identified
205 to have significant changes in abundance in *G9a* cKO oocytes, many proteins changing in *G9a-Glp*
206 cDKO oocytes displayed the same directional trend in *G9a* cKO oocytes (**Fig. 3B**).

207 We detected five known G9A/GLP targets (ACIN1, DNMT1, DNMT3A, MTAL and RUVBL2): none of
208 these were significantly regulated in cKO oocytes; this is not entirely unexpected as protein
209 methylation does not necessarily influence abundance, but rather may affect activity. GO analysis did
210 not detect any significant enrichment terms amongst the differentially abundant proteins. Even so,

211 we identified several proteins for which change in abundance may be related to the observed oocyte
212 phenotypes. Among these, two were meiotic factors according to the MGI Gene Ontology Browser
213 (CDC25B and SIRT1), while literature research linked a further seven (STAT3, TGON1, SET, IMPDH2,
214 DSTN, SKA3, ROCK1) to meiosis in the oocyte (**Supplemental Table S2**). Furthermore, proteins involved
215 in oocyte maturation (ERMP1) and fertilization (ASTL) showed significantly increased abundance, as
216 well as oocyte transcription factor HMGB3. Increased abundance of these proteins may underlie the
217 meiotic spindle abnormalities, impaired oocyte maturation and poor fertilization rates observed in
218 *G9a-Glp* cKO oocytes. In line with observations in oocyte and embryo development, as well as H3K9
219 methylation, the more severe effect in *G9a-Glp* cDKO oocytes suggests an additional role for GLP. The
220 similar but lesser, non-significant changes in protein abundance observed in *G9a* cKO oocytes suggests
221 that the function of GLP may be compensatory of G9A, rather than unique.

222

223 **Loss of GLP results in local and distinct DNA methylation changes**

224 G9A-mediated H3K9me2 has been linked to DNA methylation (Tachibana et al. 2008; Zeng et al. 2019),
225 although genome-wide analysis only detected local DNA methylation changes in *G9a* cKO oocytes and
226 *G9a* KO embryos (Auclair et al. 2016; Au Yeung et al. 2019). To examine whether loss of GLP affects
227 DNA methylation establishment in the oocyte, we first analysed global DNA methylation (5mC and
228 5hmC) by IF. In NSN oocytes, 5mC was observed throughout the nucleus in both euchromatic and
229 heterochromatic regions (**Fig. 4A**); 5hmC was enriched in heterochromatic foci but also present in
230 euchromatin (**Fig. 4A**). No changes in localization of 5mC or 5hmC were observed in cKO oocytes.
231 However, when assessing 5mC fluorescence intensity, there were significant decreases in the *Glp* cKO
232 and *G9a-Glp* cDKO compared to control oocytes, but not for *G9a* cKO oocytes (**Fig. 4B**). No significant
233 changes in 5hmC levels were observed in cKO oocytes, although 5hmC levels also appear reduced in
234 cKO oocytes. These data suggest that *de novo* DNA methylation may be impaired upon loss of GLP but
235 not G9A in oocytes.

236 We then explored changes in DNA methylation in greater resolution by whole-genome bisulphite
237 sequencing (BS-seq) of control, *G9a* cKO and *G9a-Glp* cDKO GV oocytes. In contrast to decreased 5mC
238 seen by IF, BS-seq did not show significant global changes in DNA methylation (**Supplemental Fig.**
239 **S4A**). An explanation for this apparent discrepancy is that the genomic regions assessed by the two
240 methods differ: IF signal reports both euchromatic and heterochromatic fractions of the genome,
241 while BS-seq data is enriched in euchromatic and non-repetitive regions that can be uniquely mapped
242 and analysed. These differences highlight the value of using both methods to understand genome-
243 wide patterns of DNA methylation and may explain previous contradictory findings (Au Yeung et al.
244 2019; Zeng et al. 2019).

245 Although global DNA methylation levels as detected by BS-seq did not differ, local changes in DNA
246 methylation were analysed by binning the genome into consecutive windows of 100 CpG sites (100-
247 CpG windows). Differential methylation analysis identified 9,187 DMRs in *G9a-Glp* cDKO oocytes
248 (4.88% of all analysed 100-CpG windows), of which 4,184 (45.5%) were hypermethylated (mean
249 methylation difference: 35.1%) and 5,003 (54.5%) hypomethylated (mean methylation difference
250 25.6%) (**Fig. 4C; Supplemental Table S3**). Methylation was more affected in *G9a-Glp* cDKO than in *G9a*
251 cKO oocytes, with >7 times more DMRs identified: there were 1,252 DMRs (0.67% of all analysed 100
252 CpG windows) in the *G9a* cKO, of which 432 (34.5%) were hypermethylated (mean methylation
253 difference: 39.4%) and 820 (65.5%) hypomethylated (mean methylation difference: 33.8%)
254 (**Supplemental Fig. S4B**). Importantly, the majority of *G9a* cKO DMRs overlapped *G9a-Glp* cDKO DMRs
255 (**Supplemental Fig. 4C**). This indicates that while both G9A and GLP are required for normal DNA
256 methylation establishment in the oocyte, GLP can partially compensate for loss of G9A, but it does not
257 exclude the possibility that GLP has an additional G9A-independent role in DNA methylation.

258 To assess this possibility in more detail, we analysed the regions of the genome affected by DNA
259 methylation changes. While hypermethylated DMRs show similar overlap with genic and intergenic
260 regions, hypomethylated DMRs are enriched in genic regions (**Supplemental Fig. S4D**). This is

261 expected, as hypomethylated DMRs are found in regions that are methylated in control oocytes and
262 it is well established that DNA methylation localises to transcribed genes in oocytes (Veselovska et al.
263 2015). To assess whether DNA methylation changes correlate with underlying histone modifications,
264 we tested the overlap of DMRs with H3K9me2, H3K27me3 and H3K4me3 (**Fig. 4D**). The majority of
265 DMRs did not overlap regions with H3K9me2 and there was no clear distinction between hyper- and
266 hypomethylated DMRs, indicating that most DNA methylation changes in cKO oocytes are unlikely to
267 be a direct consequence of loss of H3K9me2. Interestingly, hypermethylated DMRs were strongly
268 enriched for H3K27me3, compared to hypomethylated DMRs. Importantly, this enrichment was not
269 seen for H3K4me3, although both are enriched in regions of the genome lacking DNA methylation.
270 Because H3K27me3 and DNA methylation are mutually exclusive, this result may indicate a localised
271 redistribution of the two marks in cKOs.

272 Since G9A and GLP can interact with UHRF1 (Kim et al. 2009; Ferry et al. 2017), we also investigated
273 the overlap of DMRs with regions that are hypomethylated in *Uhrf1* cKO oocytes (Maenohara et al.
274 2017). *Uhrf1* cKO oocytes show widespread hypomethylation, and we observed that both *G9a* cKO
275 and *G9a-Glp* cDKO hypomethylated DMRs strongly overlap with *Uhrf1* hypomethylated regions
276 compared to random and random methylated probes (**Fig. 4E**). These data support that loss of G9A
277 and GLP may disturb a subset of UHFR1-mediated methylation.

278 Between 21 and 38% of 100-CpG windows identified as DMRs cluster and form larger regions that, in
279 both genotypes, can span genes (**Fig. 4E**, **Supplemental Fig. S4E-G** and **Supplemental Table S3)**. In
280 total, there were 707 hypo- and 869 hyper-methylated domains in *G9a-Glp* cDKO oocytes, with fewer
281 in the *G9a* cKO (140 hypo- and 66 hyper-methylated domains). To see whether the additional changes
282 in the *G9a-Glp* cDKO are unique or whether similar (non-significant) trends are present in the *G9a*
283 cKO, we performed unsupervised cluster analysis of DNA methylation of the cDKO domains (**Fig. 4F**).
284 For both hypo- and hypermethylated domains, we identified domains common to both cKOs (523
285 hypo, 590 hyper) and domains unique to the *G9a-Glp* cDKO (229 hypo, 279 hyper; **Fig. 4F,G;**

286 **Supplemental Fig. S4E-G**). This indicates that the majority of effects seen in the *G9a-Glp* cDKO are also
287 present in the *G9a* cKO, although to a lower, often non-significant magnitude. Furthermore, there
288 appears to be a potentially unique role of GLP in oocyte DNA methylation, although this is likely to be
289 minor compared to its function compensatory to loss of G9A.

290

291 **Transcriptome changes direct DNA methylation and protein changes in *G9a-Glp* cDKO oocytes**

292 We evaluated gene expression changes by RNA-seq in *G9a-Glp* cDKO, *G9a* cKO and matched control
293 GV oocytes. Differential gene expression was determined by DESeq2 analysis followed by filtering for
294 genes with $Log_2FC>1.5$. The vast majority of differentially expressed genes (DEGs) were upregulated
295 in the *G9a-Glp* cDKO. Again, *G9a-Glp* cDKO oocytes were more severely affected than *G9a* cKO
296 oocytes, with 330 DEGs (301 up, 29 down; **Fig. 5A, Supplemental Table S4**), in contrast to 79 DEGs in
297 *G9a* cKO oocytes (64 up, 15 down; **Supplemental Fig. S5A**). Of the *G9a* cKO DEGs, 51 overlapped with
298 *G9a-Glp* cDKO DEGs. Clustering analysis identified three clusters: 1) downregulated in both *G9a* cKO
299 and *G9a-Glp* cDKO; 2) upregulated in both genotypes; and 3) uniquely upregulated in *G9a-Glp* cDKO
300 (**Fig. 5B**). GO analysis did not show significant category enrichments, but amongst the deregulated
301 transcripts we identified several transcription factors with a known function in the oocyte (*Prmt7,*
302 *Etv5*), zygotic genome activation (*Zscan4d*) and embryo development (*Klf4, Hoxd1, Lmx1a*;
303 **Supplemental Table S4**). Furthermore, several genes important for oocyte maturation, meiosis and
304 fertilization were deregulated (*Atrx, Fgfr2, Prkcq, Ptgs2, Plac1, Mt1*), which may underlie some of the
305 phenotypic effects we see.

306 Both our proteome and transcriptome analysis showed a preferential upregulation of protein and
307 transcript abundance in *G9a-Glp* cDKO oocytes, respectively. To assess whether changes in transcript
308 expression may be causative for changes in protein abundance, we used gene set enrichment analysis
309 (**Fig. 5C**). Indeed, proteins with increased abundance were enriched for transcriptionally upregulated
310 genes in *G9a-Glp* cDKO oocytes, whereas proteins with decreased abundance were enriched for

311 downregulated genes, although this may not account for all the variation in protein abundance. This
312 indicates that loss of GLP results in deregulated gene expression, which in turn affects abundance of
313 the corresponding proteins. Hence, although the majority of genes appear unaffected by loss of GLP,
314 the transcriptional changes that do occur are likely to be of biological significance.

315 Using the DEG clusters, we assessed the overlap of DEGs with the distribution of histone modifications
316 (**Supplemental Fig. S5B**). There was no significant enrichment for any of the clusters with H3K9me2,
317 further supporting that H3K9me2 does not correlate with transcriptional repression in the oocyte
318 (**Supplemental Fig. S3C**). Interestingly, similar to hypermethylated DMRs, upregulated DEGs (clusters
319 2 and 3) were enriched in H3K27me3. As transcription is linked to the deposition of gene body DNA
320 methylation in the mouse oocyte, we analysed the correlation between expression and DNA
321 methylation changes. Consistently, expression changes of DEGs positively correlated with gene-body
322 DNA methylation changes in *G9a-Glp* cDKO oocytes (**Fig. 5D**). In contrast, when evaluating genes with
323 differential methylation, the correlation was much weaker (**Supplemental Fig. S5C**). These trends
324 were similar in *G9a* cKO oocytes (**Supplemental Fig. S5D,E**). This shows that the transcriptional
325 changes observed in *G9a-Glp* cDKO oocytes impact the associated genic DNA methylation; however,
326 this association does not explain the majority of DNA methylation changes seen in *G9a-Glp* cDKO
327 oocytes, thus other mechanisms likely underlie the majority of changes observed.

328

329 ## Discussion

330 Our present study shows that GLP can partially compensate for loss of G9A and additionally has a G9A-
331 independent role in oogenesis. We find that GLP is required for oocyte maturation, meiosis and
332 developmental competence. Few embryos derived from *Glp* cKO oocytes implant and those that do
333 die mid-gestation. In contrast, maternal *G9a* cKO embryos are less affected and some develop
334 normally into healthy pups. This difference in severity is also reflected at a molecular level in gene
335 expression, protein abundance and DNA methylation. Importantly, the differences between the

336 genotypes are independent of GLP's function as an H3K9me2 methyltransferase, as H3K9me2 was
337 equally ablated in all. Therefore, we propose that the phenotypes arise from multiple mechanistic
338 changes in histone modifications, transcriptional regulation and DNA methylation, summarized in
339 **Fig. 6**.

340 To consider the molecular mechanisms underlying the observed phenotypes, it is important to
341 appreciate that G9A and GLP are proteins with multiple functions. Although best known as histone
342 methyltransferases, they can methylate and alter the function of non-histone proteins (Shinkai and
343 Tachibana 2011; Scheer and Zaph 2017). Nevertheless, the strong correlation we observed between
344 changes in transcript and protein abundance in *G9a* and *G9a/Glp* cKO oocytes supports that the
345 changes in protein abundance are likely attributable to altered genomic regulation rather than
346 G9A/GLP directly modulating protein stability. Loss of G9A and GLP resulted in transcriptional
347 upregulation, supporting previous reports that G9A/GLP act as repressors (Tachibana et al. 2002;
348 Tachibana et al. 2005). It is unlikely that this can be attributed mostly to loss of H3K9me2, because
349 only a fraction of genes was upregulated despite almost complete ablation of H3K9me2, and because
350 of the significant transcriptional differences between the *G9a* cKO and *G9a-Glp* cDKO despite similar
351 deficits in H3K9me2. Alternatively, the effects may be mediated indirectly by G9A/GLP modulating
352 activity of transcriptional repressors or through other chromatin changes. We also observed
353 upregulation of some developmental transcription factors, suggesting that some gene expression
354 changes reflect illegitimate expression of such factors in oocytes. The more extensive transcriptional
355 deregulation in the *G9a-Glp* cDKO is associated with impaired developmental capacity of the oocyte,
356 resulting in decreased oocyte maturation, meiotic spindle abnormalities, impaired fertilization and
357 abnormal embryo development.

358 G9A and GLP have been linked to DNA methylation in multiple studies. In the embryo, loss of G9A
359 leads to hypomethylation of a subset of CGI promoters (Auclair et al. 2016). In the oocyte, we and
360 others do not see widespread hypomethylation, but instead local sites of hypo- and hypermethylation

361 (Au Yeung et al. 2019). A variety of mechanisms could cause these changes. In the oocyte, *de novo*
362 DNA methylation requires transcription (Kobayashi et al. 2012; Veselovska et al. 2015). The
363 transcriptional changes in *G9a* cKO and *G9a-Glp* cDKO oocytes correlate with DNA methylation
364 changes, indicating that upregulated gene expression is responsible for some of the hypermethylation
365 observed. However, the significant localisation of *G9a* cKO and *G9a-Glp* cDKO hypermethylated
366 regions with H3K27me3 suggests that the loss of G9A/GLP may impair the repressive chromatin
367 landscape in the oocyte, either through H3K9me2 or modulation of a transcriptional repressor.
368 Conversely, a large subset of hypomethylated DMRs overlapped with regions that are hypomethylated
369 in *Uhrf1* cKO oocytes (Maenohara et al. 2017). UHRF1 function has been associated with G9A and GLP
370 in several ways, either by direct interaction (Kim et al. 2009) or indirect recruitment through
371 H3K9me2/3 or LIG1 (Rothbart et al. 2012; Rothbart et al. 2013; Ferry et al. 2017). However, it is not
372 clear how these mechanisms apply in the oocyte because of the absence of DNA replication. Although
373 UHRF1 appears to be required for some genomic DNA methylation, loss of DNMT1 has only minor
374 effects, largely through a role in ensuring symmetric methylation of *de novo* methylated CpGs (Shirane
375 et al. 2013; Maenohara et al. 2017). There are likely other mechanisms besides transcriptional
376 regulation and UHRF1 interactions at play in the *G9a* cKO and *G9a-Glp* cDKO oocytes. These include
377 the possibility of a direct interaction of G9A and GLP with DNMT proteins. For example, G9A and GLP
378 can dimethylate DNMT3A at lysine 44. Methylated DNMT3A can be bound by MPP8, which in turn
379 binds automethylated GLP, resulting in a DNMT3A-MPP8-GLP silencing complex (Chang et al. 2011).

380 In contrast to previous reports (Tachibana et al. 2005), we saw that while H3K9me2 depends on both
381 G9A and GLP, the persistence of GLP in the *G9a* cKO was sufficient to establish H3K9me1. Notably,
382 loss of G9A and GLP did not completely eliminate H3K9me1, indicating that other methyltransferases,
383 such as PRDM3 and PRDM16, may be active in the oocyte. It remains unclear whether the decrease in
384 H3K9me1 may be (partially) causative for the transcriptional and DNA methylation changes: so far,
385 H3K9me1 has not been associated with either but rather is proposed to be predominantly a substrate
386 for H3K9 di- and trimethylation (Pinheiro et al. 2012).

387 It is difficult to distinguish between a compensatory effect and a unique role for GLP in the oocyte.
388 When comparing transcription, protein and DNA methylation data from *G9a* cKO and *G9a-Glp* cDKO
389 oocytes, some genes/proteins/regions are progressively affected while others only affected in *G9a-*
390 *Glp* cDKO oocytes. The possibility of a unique, G9A-independent role for GLP is supported by a recent
391 study in zygotes, where GLP interacts with PRC2 to establish H3K27me2 in the paternal pronucleus
392 (Meng et al. 2020). In our models, the unique function was especially apparent in the transcriptome,
393 where genes with the greatest fold-change where unique to the *G9a-Glp* cDKO. The upregulation seen
394 in most DEGs was reflected in an upregulation of protein abundance in *G9a-Glp* cDKO oocytes,
395 indicating that although only a relatively small proportion of genes is derepressed upon loss of G9A
396 and GLP, the transcriptional changes are likely to have a functional impact in the oocyte. Indeed, we
397 saw changes in gene expression and protein abundance of several genes related to oocyte maturation,
398 meiosis and fertilization. Taken together, our results highlight GLP as a multi-functional protein
399 involved in different regulatory processes in the oocyte. They show that it has a unique role that is
400 critical for the developmental capacity of the oocyte and independent of G9A and its role as H3K9me2
401 methyltransferase.

402

403 ## Materials and methods

404 **Sample collections**

405 All experimental procedures were performed under licences issued by the Home Office (UK) in
406 accordance with the Animals (Scientific Procedures) Act 1986 and were approved by the Animal
407 Welfare and Ethical Review Body at the Babraham Institute.

408 Oocytes and embryos were collected in M2 medium (Sigma-Aldrich, M7167) unless stated otherwise.
409 GV and MII oocytes for IF analysis were collected from adult mice aged ~12 weeks and fixed in 2% PFA
410 for 15 minutes. MII oocytes were collected after superovulation. Oocytes used for ChIP-seq, BS-seq

411 and RNA-seq were collected from ovaries of 22-26 day-old mice using a collagenase/trypsin digest.
412 For ChIP-seq, 300 GV oocytes were collected in nuclear lysis buffer and pooled from two to four mice
413 for each replicate. For BS-seq and RNA-seq, replicates were stored in RLT+ buffer (Qiagen). Each
414 replicate comprised all oocytes collected from one mouse (75-200 GV oocytes). For whole-proteome
415 analysis oocytes were collected from ovaries of 22-26 day-old mice. To avoid contamination with
416 proteins/peptides from the medium, oocytes were collected by manual dissection of ovaries in
417 protein-free L15 medium (Thermo Fisher Scientific, 31415029). ~200 GV oocytes were collected from
418 two mice in parallel, washed 3 times in PBS with 1x cOmplete Protease Inhibitor Cocktail (Merck,
419 11697498001).

420 Preimplantation embryos were collected after natural mating of control and cKO females with
421 C57BL/6Babr WT males at E0.5 or E3.5. Implantation was determined by counting the number of
422 implantation sites in uteri at E6.5 after timed mating. To score postimplantation development,
423 embryos were collected after natural mating at E8.5 and E12.5. For embryo culture, female mice were
424 superovulated and embryos dissected in M2 medium at E1.5 after natural mating with WT males.
425 Fertilized embryos (1-cell and 2-cell stage) were selected for culture in M16 medium (Sigma-Aldrich,
426 MR-016-D) under mineral oil (Sigma-Aldrich, M8410) at 37°C and 5% CO_2 for 3 days, and
427 developmental progress recorded each day.

428 **Immunofluorescence analysis**

429 IF was performed after antibody staining as previously described (Santos et al. 2003). Primary
430 antibodies are listed in **Supplemental Table S5**. Samples were analysed on a Zeiss LSM780 confocal
431 microscope (63x oil-immersion objective). Single optical sections were captured and semi-
432 quantification of fluorescence intensity was performed using Volocity 6.3 (Improvision).

433 **LC-MS proteome analysis**

434 Oocytes were lysed in 20µl dissolution buffer containing 100mM triethylammonium bicarbonate
435 (Sigma, T4708) and 0.1% Sodium Dodecyl Sulfate (SDS), followed by water bath sonication and boiling
436 at 90℃ for 5min. Proteins were reduced with tris-2-carboxyethyl phosphine (TCEP, Sigma) for 1h at
437 60℃ at a final concentration of 5mM, followed by cysteine blocking for 10min at room temperature
438 using methyl methanethiosulfonate (MMTS, Sigma) at final concentration of 10mM. Samples were
439 digested overnight at 37℃ with trypsin (Pierce #90058) and the next day peptides were labelled with
440 TMT11plex reagents (0.4mg per sample) according to manufacturer's instructions (Thermo Scientific).
441 To quench the reaction, 3µl of 5% hydroxylamine (Thermo Scientific) was added for 15min and
442 samples combined and dried with centrifugal vacuum concentrator. The TMT mix was fractionated
443 with Reversed-Phase spin columns at high pH (Pierce #84868). Nine fractions were collected using
444 different elution solutions in the range of 5–50% ACN and were analysed on a Dionex UltiMate 3000
445 UHPLC system coupled with the nano-ESI Fusion-Lumos (Thermo Scientific) mass spectrometer.
446 Samples were loaded on the Acclaim PepMap 100, 100µm × 2cm C18, 5µm, 100Å trapping column
447 with the ulPickUp injection method at loading flow rate 5µl/min for 10 min. For peptide separation,
448 the EASY-Spray analytical column 75µm × 25cm, C18, 2µm, 100 Å column was used for multi-step
449 gradient elution. Full scans were performed in the Orbitrap in the range of 380-1500 m/z at 120K
450 resolution and peptides isolated in the quadrupole with isolation window 1.2Th, HCD collision energy
451 38% and resolution 50K. Raw data were processed with the SequestHT search engine in Proteome
452 Discoverer 2.1 software and searched against a Uniprot database containing mouse reviewed entries.
453 The parameters for the SequestHT node were: Precursor Mass Tolerance 20ppm, Fragment Mass
454 Tolerance 0.02Da, Dynamic Modifications were Oxidation of M (+15.995Da), Deamidation of N, Q
455 (+0.984Da) and Static Modifications were TMT6plex at any N-Terminus, K (+229.163Da) and
456 Methylthio at C (+45.988Da). The consensus workflow included TMT signal-to-noise (S/N) calculation
457 and the level of confidence for peptide identifications was estimated using the Percolator node with
458 decoy database search. Strict FDR was set at q-value<0.01. For downstream data analysis, the R
459 package qPLEXanalyzer was used (Papachristou et al. 2018). The mass spectrometry proteomics data

460 have been deposited to the ProteomeXchange Consortium via the PRIDE partner repository (Perez-
461 Riverol et al. 2019) with the dataset identifier PXD030265.

462 **Preparation of sequencing libraries**

463 ChIP-seq libraries were prepared using ULI-nChIP as previously described (Hanna et al. 2018b).
464 Antibodies were added at 250ng/reaction for both anti-H3K9me2 (mouse monoclonal, Abcam,
465 ab1220) and anti-IgG (rabbit polyclonal, Diagenode, EB-070-010). Library preparation was completed
466 with a MicroPlex Library Preparation kit v2 (Diagenode) with Sanger 8-base indices for multiplexing.
467 Relative enrichment over input was quantified using the library concentrations determined by
468 Bioanalyzer High Sensitivity DNA Analysis (Agilent). Low input bisulphite (BS)-seq libraries were
469 prepared by post-bisulphite adapter tagging as previously described (Hanna et al. 2018b). RNA-seq
470 libraries were prepared as described (Hanna et al. 2019).

471 **Sequencing and data processing**

472 Libraries were sequenced on Illumina MiSeq, HiSeq2500 and NextSeq500 systems. ChIP-seq libraries
473 were sequenced to an average of 57 million paired-end reads of 75 bp read-length (**Supplemental**
474 **Table S5**). BS-seq libraries were sequenced to an average of 16 million paired-end reads for *G9a* cKO
475 and 26 million reads for *G9a-Glp* cDKO oocytes of 100-125 bp read-length. RNA-seq libraries were
476 sequenced to an average single read number of 1.9 million for *G9a* cKO and *G9a-Glp* cDKO oocytes of
477 50 bp read-length. Raw fastq files were processed with Trim Galore, then mapped to the mouse
478 GRCm38 genome. Mapping of ChIP-seq data was done using Bowtie2, RNA-seq data by Hisat2 v2.1.0
479 guided by known splice sites, BS-seq data with Bismark v0.19.0.

480 **Sequencing data analysis**

481 Sequencing data analysis was conducted using SeqMonk
482 (https://www.bioinformatics.babraham.ac.uk/projects/seqmonk/). For ChIP-seq analysis, 10kb
483 running windows (*N*=272,566) were quantified as reads per kilobase per million (RPKM). Windows

484 were filtered to exclude mapping artefacts, defined as RPKM>6 in at least one replicate set of 10%
485 input libraries (*N*=408). H3K9me2 enrichment was defined as Log_2RPKM>2.5 in d25 GV oocytes
486 (*N*=34,192). A set of random windows was sampled from all 10kb windows (*N*=35,000). H3K9me2-
487 enriched and random windows were then merged with adjacent windows within 10kb, resulting in
488 12,154 H3K9me2-enriched domains and 26,077 random domains. Genic and intergenic regions were
489 defined as overlapping or not overlapping oocyte transcripts, respectively, and promoters were
490 defined as +/-500bp around transcription start sites of oocyte transcripts (Veselovska et al. 2015). CGIs
491 were defined as previously described (Illingworth et al. 2008). Oocyte transcription levels were
492 categorized into not expressed (FPKM<0.1), low expressed (FPKM 0.1-1) and high expressed (FPKM>1)
493 using published data (Veselovska et al. 2015).

494 BS-seq data were analysed using a tile-based approach of 100 CpGs for each consecutive genome
495 window, ensuring equal CpG content in all windows analysed. Methylation values were quantified
496 using the bisulphite-sequencing pipeline quantification, which calculates per-base methylation
497 percentages and averages these within each window. Filters were applied to ensure a minimum
498 coverage of ≥10 observed cytosines per window. Only windows with this minimal coverage in all
499 samples were taken into account, allowing assessment of 86.2% of 100 CpG windows (*N*=188,433).
500 Differentially methylated regions (DMRs) were defined by statistical comparison of DNA methylation
501 levels for each 100 CpG window between control and *G9a* cKO or control and *G9a-Glp* cDKO oocytes
502 using the EdgeR function in SeqMonk. To assess overlap of DMRs with genomic features, CGI and
503 oocyte gene annotations were used from (Veselovska et al. 2015). DMRs were merged to form
504 differentially methylated domains (DMDs). Hierarchical clustering analysis of DMDs was performed in
505 R using Euclidean distance and Ward's agglomeration method as implemented by the package
506 pheatmap.

507 For analysis of RNA-seq data, expression of oocyte genes (Veselovska et al. 2015) was quantified using
508 log transformed read count quantitation per million reads. Differential gene expression was analysed

509 using DESeq2 followed by filtering of genes with $Log_2FC>1.5$. Clustering analysis of DEGs was
510 performed in R using Euclidean distance and Ward's agglomeration method. Relative enrichment of
511 differentially abundant proteins amongst DEGs was displayed using the barcode method from the
512 Limma R package. The ranked list of expression changes only considered genes corresponding to
513 proteins identified in the proteome. Spearman's rank correlation coefficient between DNA
514 methylation difference and expression log_2FC was used to interrogate the relationship between DNA
515 methylation and transcriptional changes.

516 Sequencing data were submitted to the GEO under accession number GSE191026. Publicly available
517 ChIP-seq and BS-seq data under accessions GSE93941, DRA005849 were used to develop our studies.

518 **Statistical analysis**

519 Statistical analysis was conducted in Graphpad Prism, R and VassarStats. SN proportion was compared
520 using two-way ANOVA (Stage x Genotype) with Šídák's multiple comparisons test. Proportion of
521 embryo stage at E3.5, number of implantation sites at E6.5 and mean fluorescence intensity of
522 confocal IF images were analysed using one-way ANOVA with Tukey's posthoc test. Litter sizes were
523 compared using a nested one-way ANOVA with mouse as nested factor. A χ-square test was used to
524 analyse frequency of overlap of genic/intergenic regions with DMRs, histone modifications with DMRs,
525 Uhrf1 hypomethylated regions with DMRs and DEGs with histone modifications. *P*-value was adjusted
526 using Bonferroni correction to control for multiple comparisons.

527

528 ## Figure legends

529 **Figure 1. Developmental potential of *G9a* cKO, *Glp* cKO and *G9a-Glp* cDKO oocytes.**

530 **A)** Representative images showing IF for G9A and GLP in NSN oocytes. Scale bar: 20 µm.

531 **B)** Stacked bar chart showing percentage of NSN, intermediate and SN oocytes from mice aged 12
532 weeks. Number of mice: Control=5, *G9a* cKO=3, *Glp* cKO=2, *G9a-Glp* cDKO=3. Ctrl *vs. G9a* cKO:

533 *P=0.7667*; Ctrl *vs Glp* cKO: *P= 0.0075*; Ctrl *vs G9a-Glp* cDKO: *P<0.0001*; *G9a* cKO *vs G9a-Glp* cDKO
534 *P=0.0058.*
535 **C)** Bar charts showing percentage of chromosome misalignments and spindle abnormalities in MII
536 oocytes. Dots represent datapoints from single mice. Examples of normal and abnormal spindles
537 are shown in IF images below. *G9a* cKO: *P=0.7037*; *Glp* cKO: *P=0.0678*; *G9a-Glp* cDKO: *P=0.0670.*
538 **D)** Stacked bar chart showing developmental stage (%) of embryos from cKO females mated with WT
539 males and collected on E3.5. Number of mice: Control=5, *G9a* cKO=5, *Glp* cKO=6, *G9a-Glp* cDKO=6.
540 Blastocysts: Ctrl *vs G9a* cKO *P*=0.9939; Ctrl *vs Glp* cKO *P*=0.0761, Ctrl *vs G9a-Glp* cDKO *P=0.0073*;
541 One-cell stage: Ctrl *vs G9a-Glp* cDKO *P=0.0406.*
542 **E)** Bar chart showing number of implantation sites scored at E6.5. Dots represent single mice. Ctrl *vs*
543 *Glp* cKO *P*=0.0093; Ctrl *vs G9a-Glp* cDKO *P*=0.0020.
544 **F)** Boxplots showing average litter size of females with cKO oocytes mated with WT males. Number
545 of mice: Control=9, *G9a* cKO=5, *Glp* cKO=3, *G9a-Glp* cDKO=3; Number of litters: Control=60, *G9a*
546 cKO=26, *Glp* cKO=0, *G9a-Glp* cDKO=0; Ctrl *vs G9a* cKO: *P=0.0087.*
547
548 **Figure 2. Analysis of H3K9 methylation in *G9a* cKO, *Glp* cKO and *G9a-Glp* cDKO oocytes.**
549 **A)** Representative IF images of NSN oocytes for H3K9me1, H3K9me2 and H3K9me3 in control, *G9a*
550 cKO, *Glp* cKO and *G9a-Glp* cDKO oocytes.
551 **B)** Boxplots of quantitation of IF images. Dots represent individual oocytes. Analysis is based on 2-5
552 mice per genotype and 3-4 replicate experiments for each antibody.
553 **C)** Genome screenshot showing H3K9me2 enrichment as determined by ChIP-seq in WT oocytes
554 from mice aged 15 and 25 days. Y-axis scaling represents RPKM. Annotation tracks highlight oocyte
555 transcripts, CpG islands, oocyte DNA methylated and unmethylated domains, and H3K9me2-
556 enriched domains (Log_2RPKM>2.5 in d25 GV oocytes).
557 **D)** Boxplots showing relative enrichment over input of H3K9me2 ChIP-seq libraries. Dots represent
558 individual samples.

559 **E)** PCA plot of H3K9me2 (blue shading), input (green shading) and IgG (yellow shading) ChIP-seq
560 libraries, comparing WT (d15 and d25), control, *G9a* cKO and *G9a-Glp* cDKO samples.
561 **F)** Probe trend plot showing loss of H3K9me2-enrichment in *G9a* cKO and *G9a-Glp* cDKO oocytes
562 compared to WT and control oocytes in H3K9me2-enriched domains but not random domains.
563

564 **Figure 3. Proteome analysis of *G9a* cKO and *G9a-Glp* cDKO oocytes.**

565 **A)** GO analysis of the oocyte proteome.
566 **B)** Volcano plot showing differential abundance of proteins in *G9a* cKO oocytes compared to
567 controls. Significantly changing proteins ($P<0.05$ and $Log_2FC>0.3$) are highlighted in dark blue
568 (decreased abundance) or dark red (increased abundance); light blue and light red dots indicate
569 proteins changing significantly in cDKO oocytes.
570 **C)** Volcano plot showing differential abundance of proteins in *G9a-Glp* cDKO oocytes compared to
571 controls. Significantly changing proteins ($P<0.05$ and $Log_2FC>0.3$) are highlighted in dark blue
572 (decreased abundance) or dark red (increased abundance). Light blue and light red dots indicate
573 proteins changing significantly in *G9a* cKO oocytes. Proteins changing significantly and with oocyte
574 function of interest are labelled.
575 **D)** Venn diagram of significant changing proteins in *G9a* cKO and *G9a-Glp* cDKO oocytes.
576

577 **Figure 4. DNA methylation changes in *G9a* cKO and *G9a-Glp* cDKO oocytes.**

578 **A)** Representative IF images of NSN oocytes showing 5mC and 5hmC in Control, *G9a* cKO, *Glp* cKO
579 and *G9a-Glp* cDKO oocytes.
580 **B)** Boxplots of quantitation of IF images. Dots represent individual oocytes. Analysis is based on 2
581 mice per genotype and 2 replicate experiments for each antibody.
582 **C)** Scatterplot showing methylation levels of 100-CpG windows in control vs *G9a-Glp* cDKO oocytes.
583 Unique cDKO DMRs are highlighted in blue, DMRs shared with *G9a* cKO oocytes in red.

584 **D)** Barchart showing percentage overlap of DMRs and random probes with H3K9me2, H3K37me3
585 and H3K4me3. H3K9me2: *G9a* cKO hyper *adj. P*=0.0136, *G9a* cKO hypo *P<0.0001, G9a-Glp* cDKO
586 hypo *P<0.0001*; H3K27me3: *G9a* cKO hyper *P<0.0001, G9a-Glp* cDKO hyper *P<0.0001*; H3K4me3:
587 all genotypes *P<0.0001*.
588 **E)** Barchart showing percentage overlap of DMRs with 100-CpG windows that are hypomethylated
589 in *Uhrf1* cKO oocytes (>20% methylation difference, (Maenohara et al. 2017)), random 100-CpG
590 windows and 100-CpG windows that are highly methylated (>75%) in WT and *Uhrf1* cKO oocytes.
591 *G9a* cKO hyper *adj. P=0.0404*, *G9a-Glp* cDKO hyper, *G9a* cKO hypo and *G9a-Glp* cDKO hyper
592 *P<0.0001*.
593 **F)** Genome screenshot showing example of a region uniquely hypomethylated in *G9a-Glp* cDKO
594 oocytes spanning the *Arhgef10l* transcript. Annotation tracks show position of H3K9me2-enriched
595 domains and oocyte transcripts.
596 **G)** Heatmap showing clustering analysis of *G9a-Glp* cDKO hypo- and hypermethylated domains.
597
598 **Figure 5. Transcription changes in *G9a-Glp* cDKO oocytes in relation to protein and DNA methylation**
599 **changes.**
600 **A)** Scatterplot showing expression levels in control vs. *G9a-Glp* cDKO oocytes. Unique cDKO DEGs are
601 highlighted in blue, DEGs with $Log_2FC>1.5$ in red and DEGs shared with *G9a* cKO oocytes in green.
602 **B)** Heatmap showing relative expression levels (RPKM) of up- and down-regulated *G9a-Glp* cDKO
603 DEGs that overlap with *G9a* cKO DEGs.
604 **C)** Plot showing link between changes in transcript and protein abundance. The X-axis shows Log_2FC
605 (Control vs. *G9a-Glp* cDKO) of genes present in both transcriptome and proteome datasets
606 (*N*=2933). Blue and red boxes represent down- and up-regulated transcripts, respectively, with a
607 FC>1.5 ($Log_2FC>0.585$). Vertical blue and red lines represent differentially abundant proteins
608 (*P*<0.05 and $Log_2FC>0.3$; ten proteins not detected in the RNA-seq data are not represented).
609 Enrichment scores, shown above and below, show that downregulated proteins are enriched

610 among downregulated transcripts and upregulated proteins enriched among upregulated
611 transcripts (Spearman correlation R=0.43; P=2.2x10^{-9}).
612 **D)** Plot showing correlation between methylation changes (% methylation difference) and expression
613 changes (Log_2FC) of DEGs in *G9a-Glp* cDKO oocytes. Relative expression levels (RPKM) of each
614 gene are indicated by the colour scale. Spearman correlation is shown.
615
616 **Figure 6. The distinct roles of GLP and G9A in the oocyte.**
617 **A)** Summary of the developmental and molecular phenotypes of *G9a* cKO, *Glp* cKO and *G9a-Glp*
618 cDKO oocytes.
619 **B)** Proposed activities of GLP homodimers and G9A/GLP heterodimers on H3K9 methylation.
620 **C)** Interaction of GLP and/or G9A/GLP with UHRF1 could explain DNA hypomethylation in cKO and
621 cDKO oocytes.
622 **D)** Alternative chromatin changes that could contribute to gene up-regulation in *G9a* cKO and *G9a-*
623 *Glp* cDKO oocytes.
624

625 ## Competing interest statement

626 The authors declare no competing interests.
627

628 ## Acknowledgements

629 We would like to Kristina Tabbada and Nicole Forrester of the Sequencing, Simon Walker of the
630 Imaging, Simon Andrews and Felix Krueger of the Bioinformatics facilities, and members of the
631 Biological Support Unit at the Babraham Institute for excellent support. Work in G.K.'s lab was funded
632 by the UK Biotechnology and Biological Sciences Research Council (BBS/E/B/000C0423) and Medical
633 Research Council (MR/K011332/1, MR/S000437/1); H.D. was supported by a Fondecyt Postdoctorado
634 fellowship (N°3200676); C.H. was supported by a Next Generation Fellowship from the Centre for

635 Trophoblast Research. Part of the work in C.D'S.'s lab was funded by CRUK core grant (A29580)
636 awarded to the Cambridge Institute.

637 ***Author contributions:*** C.H., H.D. and G.K. conceptualised the study. H.D., F.S., E.K.P. and C.H. collected
638 the data. C.H., H.D., J.C-F., and K.K. performed data analysis. C.H., H.D. and J.C.-F. generated
639 manuscript figures. H.D. drafted the manuscript, with input from C.H., J.C.-F., E.K.P., C.D'S. and G.K.

640

641 **References**

642 Andreu-Vieyra CV, Chen R, Agno JE, Glaser S, Anastassiadis K, Stewart AF, Matzuk MM. 2010. MLL2 is
643 required in oocytes for bulk histone 3 lysine 4 trimethylation and transcriptional silencing.
644 *PLoS Biol* **8**.
645 Au Yeung WK, Brind'Amour J, Hatano Y, Yamagata K, Feil R, Lorincz MC, Tachibana M, Shinkai Y,
646 Sasaki H. 2019. Histone H3K9 Methyltransferase G9a in Oocytes Is Essential for
647 Preimplantation Development but Dispensable for CG Methylation Protection. *Cell reports*
648 **27**: 282-293 e284.
649 Auclair G, Borgel J, Sanz LA, Vallet J, Guibert S, Dumas M, Cavelier P, Girardot M, Forne T, Feil R et al.
650 2016. EHMT2 directs DNA methylation for efficient gene silencing in mouse embryos.
651 *Genome Res* **26**: 192-202.
652 Chang Y, Sun L, Kokura K, Horton JR, Fukuda M, Espejo A, Izumi V, Koomen JM, Bedford MT, Zhang X
653 et al. 2011. MPP8 mediates the interactions between DNA methyltransferase Dnmt3a and
654 H3K9 methyltransferase GLP/G9a. *Nat Commun* **2**: 533.
655 Collins RE, Northrop JP, Horton JR, Lee DY, Zhang X, Stallcup MR, Cheng X. 2008. The ankyrin repeats
656 of G9a and GLP histone methyltransferases are mono- and dimethyllysine binding modules.
657 *Nat Struct Mol Biol* **15**: 245-250.
658 Eymery A, Liu Z, Ozonov EA, Stadler MB, Peters AH. 2016. The methyltransferase Setdb1 is essential
659 for meiosis and mitosis in mouse oocytes and early embryos. *Development*.
660 Ferry L, Fournier A, Tsusaka T, Adelmant G, Shimazu T, Matano S, Kirsh O, Amouroux R, Dohmae N,
661 Suzuki T et al. 2017. Methylation of DNA Ligase 1 by G9a/GLP Recruits UHRF1 to Replicating
662 DNA and Regulates DNA Methylation. *Mol Cell* **67**: 550-565 e555.
663 Guibert S, Forne T, Weber M. 2012. Global profiling of DNA methylation erasure in mouse primordial
664 germ cells. *Genome Res* **22**: 633-641.
665 Hanna CW, Demond H, Kelsey G. 2018a. Epigenetic regulation in development: is the mouse a good
666 model for the human? *Hum Reprod Update* **24**: 556-576.
667 Hanna CW, Perez-Palacios R, Gahurova L, Schubert M, Krueger F, Biggins L, Andrews S, Colome-
668 Tatche M, Bourc'his D, Dean W et al. 2019. Endogenous retroviral insertions drive non-
669 canonical imprinting in extra-embryonic tissues. *Genome biology* **20**: 225.
670 Hanna CW, Taudt A, Huang J, Gahurova L, Kranz A, Andrews S, Dean W, Stewart AF, Colome-Tatche
671 M, Kelsey G. 2018b. MLL2 conveys transcription-independent H3K4 trimethylation in
672 oocytes. *Nat Struct Mol Biol* **25**: 73-82.
673 Illingworth R, Kerr A, Desousa D, Jorgensen H, Ellis P, Stalker J, Jackson D, Clee C, Plumb R, Rogers J
674 et al. 2008. A novel CpG island set identifies tissue-specific methylation at developmental
675 gene loci. *PLoS Biol* **6**: e22.

676 Kaneda M, Okano M, Hata K, Sado T, Tsujimoto N, Li E, Sasaki H. 2004. Essential role for de novo
677 DNA methyltransferase Dnmt3a in paternal and maternal imprinting. *Nature* **429**: 900-903.
678 Kim J, Zhao H, Dan J, Kim S, Hardikar S, Hollowell D, Lin K, Lu Y, Takata Y, Shen J et al. 2016. Maternal
679 Setdb1 Is Required for Meiotic Progression and Preimplantation Development in Mouse.
680 *PLoS Genet* **12**: e1005970.
681 Kim JK, Esteve PO, Jacobsen SE, Pradhan S. 2009. UHRF1 binds G9a and participates in p21
682 transcriptional regulation in mammalian cells. *Nucleic Acids Res* **37**: 493-505.
683 Kobayashi H, Sakurai T, Imai M, Takahashi N, Fukuda A, Yayoi O, Sato S, Nakabayashi K, Hata K,
684 Sotomaru Y et al. 2012. Contribution of intragenic DNA methylation in mouse gametic DNA
685 methylomes to establish oocyte-specific heritable marks. *PLoS Genet* **8**: e1002440.
686 Lan ZJ, Xu X, Cooney AJ. 2004. Differential oocyte-specific expression of Cre recombinase activity in
687 GDF-9-iCre, Zp3cre, and Msx2Cre transgenic mice. *Biol Reprod* **71**: 1469-1474.
688 Maenohara S, Unoki M, Toh H, Ohishi H, Sharif J, Koseki H, Sasaki H. 2017. Role of UHRF1 in de novo
689 DNA methylation in oocytes and maintenance methylation in preimplantation embryos.
690 *PLoS Genet* **13**: e1007042.
691 Meng TG, Zhou Q, Ma XS, Liu XY, Meng QR, Huang XJ, Liu HL, Lei WL, Zhao ZH, Ouyang YC et al. 2020.
692 PRC2 and EHMT1 regulate H3K27me2 and H3K27me3 establishment across the zygote
693 genome. *Nat Commun* **11**: 6354.
694 Papachristou EK, Kishore K, Holding AN, Harvey K, Roumeliotis TI, Chilamakuri CSR, Omarjee S, Chia
695 KM, Swarbrick A, Lim E et al. 2018. A quantitative mass spectrometry-based approach to
696 monitor the dynamics of endogenous chromatin-associated protein complexes. *Nat*
697 *Commun* **9**: 2311.
698 Perez-Riverol Y, Csordas A, Bai J, Bernal-Llinares M, Hewapathirana S, Kundu DJ, Inuganti A, Griss J,
699 Mayer G, Eisenacher M et al. 2019. The PRIDE database and related tools and resources in
700 2019: improving support for quantification data. *Nucleic Acids Res* **47**: D442-D450.
701 Peters AH, Kubicek S, Mechtler K, O'Sullivan RJ, Derijck AA, Perez-Burgos L, Kohlmaier A, Opravil S,
702 Tachibana M, Shinkai Y et al. 2003. Partitioning and plasticity of repressive histone
703 methylation states in mammalian chromatin. *Mol Cell* **12**: 1577-1589.
704 Pinheiro I, Margueron R, Shukeir N, Eisold M, Fritzsch C, Richter FM, Mittler G, Genoud C, Goyama S,
705 Kurokawa M et al. 2012. Prdm3 and Prdm16 are H3K9me1 methyltransferases required for
706 mammalian heterochromatin integrity. *Cell* **150**: 948-960.
707 Rice JC, Briggs SD, Ueberheide B, Barber CM, Shabanowitz J, Hunt DF, Shinkai Y, Allis CD. 2003.
708 Histone methyltransferases direct different degrees of methylation to define distinct
709 chromatin domains. *Mol Cell* **12**: 1591-1598.
710 Rothbart SB, Dickson BM, Ong MS, Krajewski K, Houliston S, Kireev DB, Arrowsmith CH, Strahl BD.
711 2013. Multivalent histone engagement by the linked tandem Tudor and PHD domains of
712 UHRF1 is required for the epigenetic inheritance of DNA methylation. *Genes Dev* **27**: 1288-
713 1298.
714 Rothbart SB, Krajewski K, Nady N, Tempel W, Xue S, Badeaux AI, Barsyte-Lovejoy D, Martinez JY,
715 Bedford MT, Fuchs SM et al. 2012. Association of UHRF1 with methylated H3K9 directs the
716 maintenance of DNA methylation. *Nat Struct Mol Biol* **19**: 1155-1160.
717 Sampath SC, Marazzi I, Yap KL, Sampath SC, Krutchinsky AN, Mecklenbrauker I, Viale A, Rudensky E,
718 Zhou MM, Chait BT et al. 2007. Methylation of a histone mimic within the histone
719 methyltransferase G9a regulates protein complex assembly. *Mol Cell* **27**: 596-608.
720 Santos F, Zakhartchenko V, Stojkovic M, Peters A, Jenuwein T, Wolf E, Reik W, Dean W. 2003.
721 Epigenetic marking correlates with developmental potential in cloned bovine
722 preimplantation embryos. *Current biology : CB* **13**: 1116-1121.
723 Schaefer A, Sampath SC, Intrator A, Min A, Gertler TS, Surmeier DJ, Tarakhovsky A, Greengard P.
724 2009. Control of cognition and adaptive behavior by the GLP/G9a epigenetic suppressor
725 complex. *Neuron* **64**: 678-691.

726 Scheer S, Zaph C. 2017. The Lysine Methyltransferase G9a in Immune Cell Differentiation and
727 Function. *Front Immunol* **8**: 429.
728 Seisenberger S, Andrews S, Krueger F, Arand J, Walter J, Santos F, Popp C, Thienpont B, Dean W, Reik
729 W. 2012. The dynamics of genome-wide DNA methylation reprogramming in mouse
730 primordial germ cells. *Mol Cell* **48**: 849-862.
731 Seki Y, Hayashi K, Itoh K, Mizugaki M, Saitou M, Matsui Y. 2005. Extensive and orderly
732 reprogramming of genome-wide chromatin modifications associated with specification and
733 early development of germ cells in mice. *Dev Biol* **278**: 440-458.
734 Shinkai Y, Tachibana M. 2011. H3K9 methyltransferase G9a and the related molecule GLP. *Genes Dev*
735 **25**: 781-788.
736 Shirane K, Toh H, Kobayashi H, Miura F, Chiba H, Ito T, Kono T, Sasaki H. 2013. Mouse oocyte
737 methylomes at base resolution reveal genome-wide accumulation of non-CpG methylation
738 and role of DNA methyltransferases. *PLoS Genet* **9**: e1003439.
739 Tachibana M, Matsumura Y, Fukuda M, Kimura H, Shinkai Y. 2008. G9a/GLP complexes
740 independently mediate H3K9 and DNA methylation to silence transcription. *EMBO J* **27**:
741 2681-2690.
742 Tachibana M, Sugimoto K, Fukushima T, Shinkai Y. 2001. Set domain-containing protein, G9a, is a
743 novel lysine-preferring mammalian histone methyltransferase with hyperactivity and specific
744 selectivity to lysines 9 and 27 of histone H3. *J Biol Chem* **276**: 25309-25317.
745 Tachibana M, Sugimoto K, Nozaki M, Ueda J, Ohta T, Ohki M, Fukuda M, Takeda N, Niida H, Kato H et
746 al. 2002. G9a histone methyltransferase plays a dominant role in euchromatic histone H3
747 lysine 9 methylation and is essential for early embryogenesis. *Genes Dev* **16**: 1779-1791.
748 Tachibana M, Ueda J, Fukuda M, Takeda N, Ohta T, Iwanari H, Sakihama T, Kodama T, Hamakubo T,
749 Shinkai Y. 2005. Histone methyltransferases G9a and GLP form heteromeric complexes and
750 are both crucial for methylation of euchromatin at H3-K9. *Genes Dev* **19**: 815-826.
751 Veselovska L, Smallwood SA, Saadeh H, Stewart KR, Krueger F, Maupetit-Mehouas S, Arnaud P,
752 Tomizawa S, Andrews S, Kelsey G. 2015. Deep sequencing and de novo assembly of the
753 mouse oocyte transcriptome define the contribution of transcription to the DNA
754 methylation landscape. *Genome biology* **16**: 209.
755 Xu Q, Xiang Y, Wang Q, Wang L, Brind'Amour J, Bogutz AB, Zhang Y, Zhang B, Yu G, Xia W et al. 2019.
756 SETD2 regulates the maternal epigenome, genomic imprinting and embryonic development.
757 *Nat Genet* **51**: 844-856.
758 Zeng TB, Han L, Pierce N, Pfeifer GP, Szabo PE. 2019. EHMT2 and SETDB1 protect the maternal
759 pronucleus from 5mC oxidation. *Proc Natl Acad Sci U S A* **116**: 10834-10841.

760

Figure 1

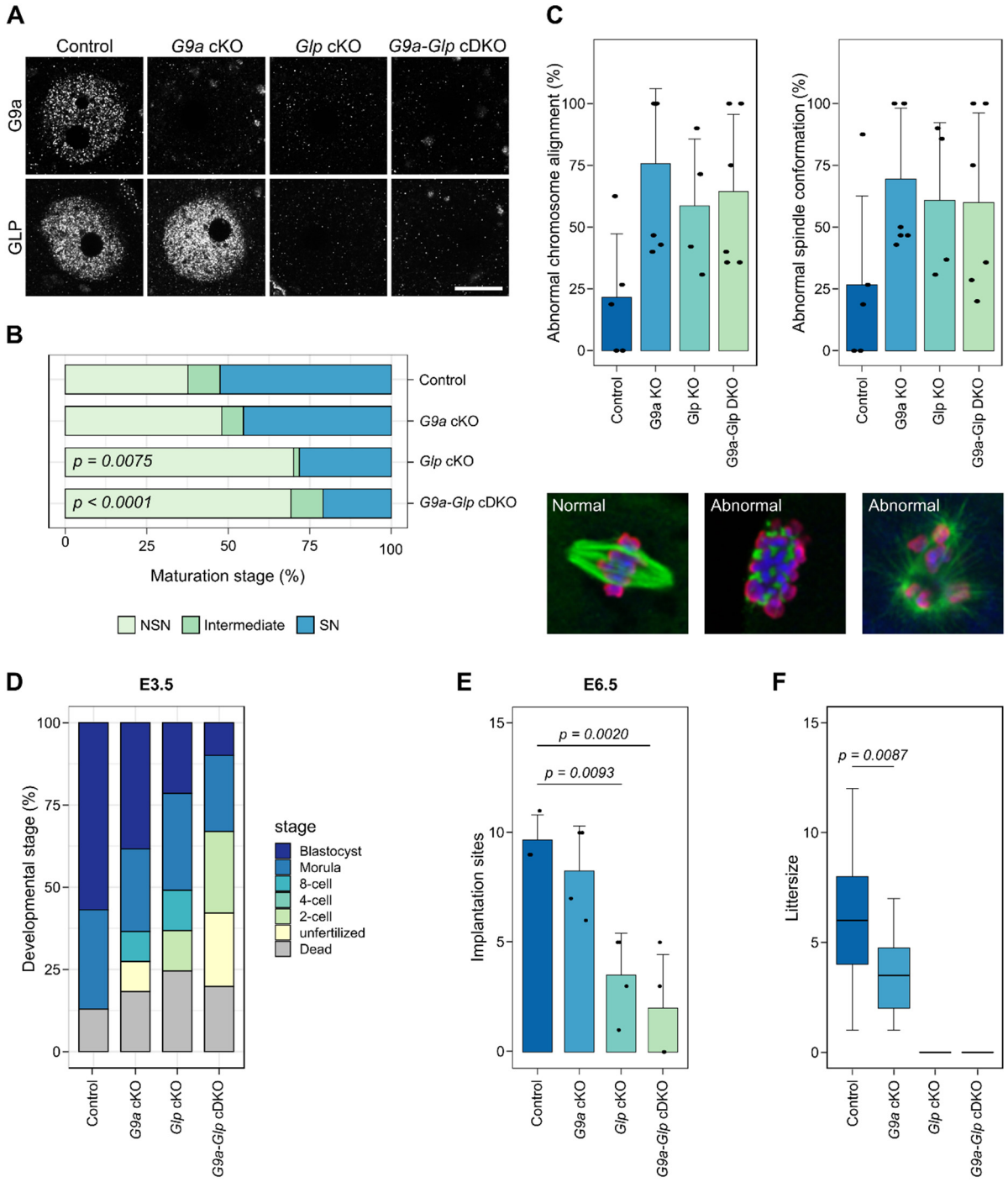
A
Control
G9a cKO
Glp cKO
G9a-Glp cDKO
G9a
GLP
B
Control
G9a cKO
Glp cKO
G9a-Glp cDKO
p = 0.0075
p < 0.0001
0
25
50
75
100
Maturation stage (%)
NSN
Intermediate
SN
C
Abnormal chromosome alignment (%)
Abnormal spindle conformation (%)
Control
G9a KO
Glp KO
G9a-Glp DKO
Normal
Abnormal
Abnormal
D
E3.5
Developmental stage (%)
stage
Blastocyst
Morula
8-cell
4-cell
2-cell
unfertilized
Dead
E
E6.5
Implantation sites
p = 0.0020
p = 0.0093
F
Littersize
p = 0.0087

Figure 2

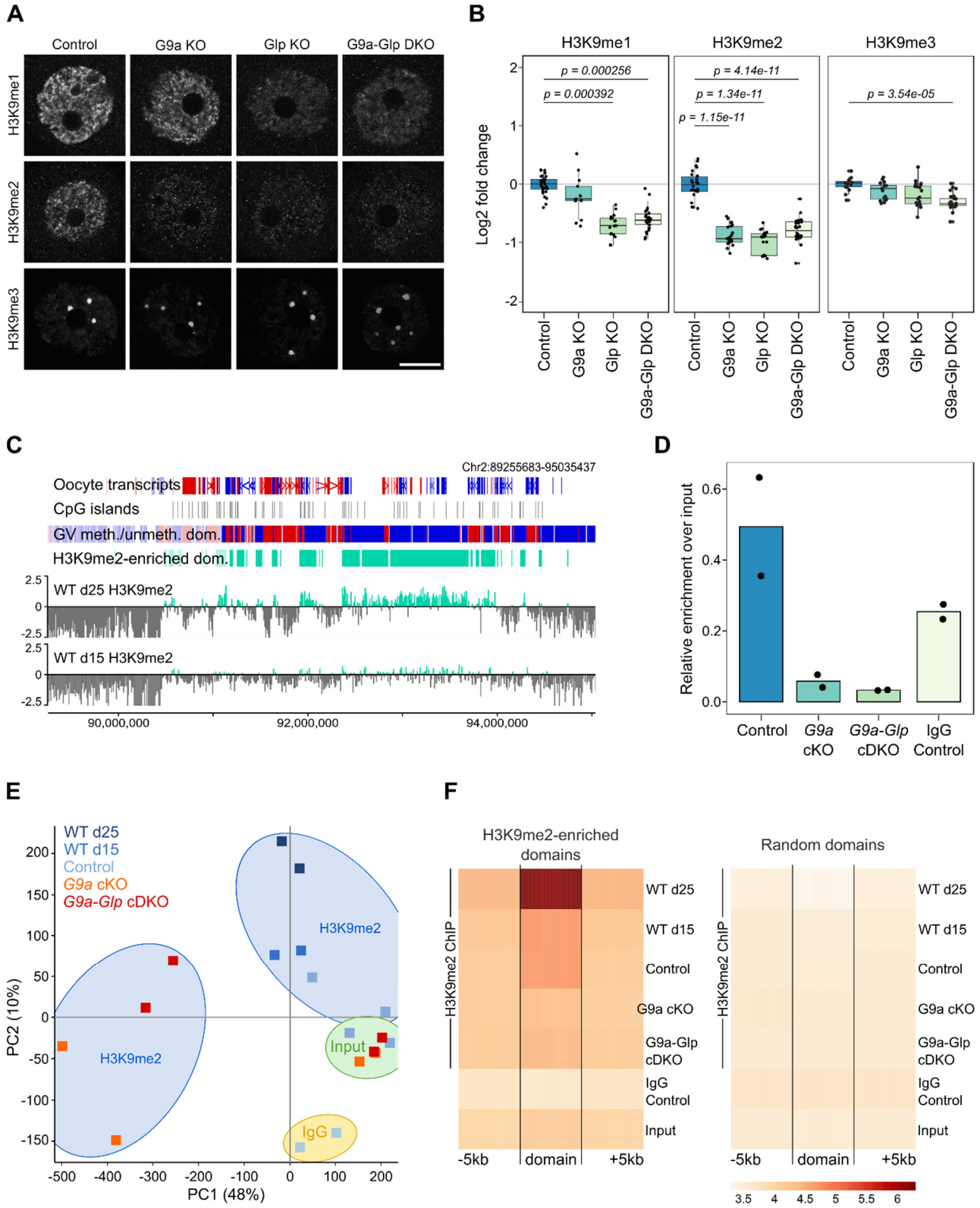
A
Control
G9a KO
Glp KO
G9a-Glp DKO
H3K9me1
H3K9me2
H3K9me3
B
H3K9me1
H3K9me2
H3K9me3
p = 0.000256
p = 0.000392
p = 4.14e-11
p = 1.34e-11
p = 1.15e-11
p = 3.54e-05
Log2 fold change
Control
G9a KO
Glp KO
G9a-Glp DKO
C
Chr2:89255683-95035437
Oocyte transcripts
CpG islands
GV meth./unmeth. dom.
H3K9me2-enriched dom.
WT d25 H3K9me2
WT d15 H3K9me2
90,000,000
92,000,000
94,000,000
D
Relative enrichment over input
Control
G9a cKO
G9a-Glp cDKO
IgG Control
E
WT d25
WT d15
Control
G9a cKO
G9a-Glp cDKO
H3K9me2
Input
IgG
PC2 (10%)
PC1 (48%)
F
H3K9me2-enriched domains
Random domains
H3K9me2 ChIP
WT d25
WT d15
Control
G9a cKO
G9a-Glp cDKO
IgG Control
Input
-5kb
domain
+5kb

Figure 3

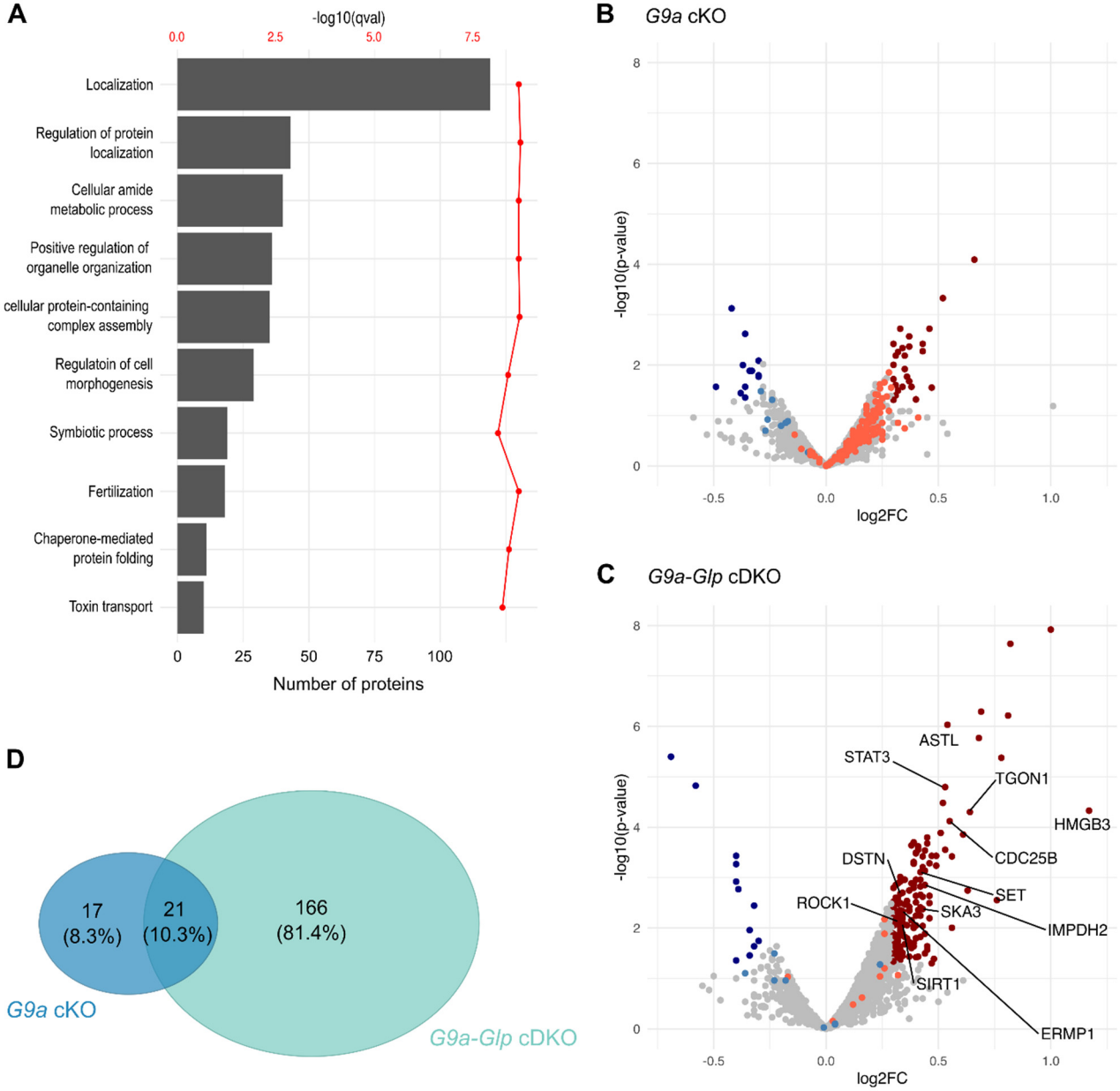
A
-log10(qval)
0.0
2.5
5.0
7.5
Localization
Regulation of protein localization
Cellular amide metabolic process
Positive regulation of organelle organization
cellular protein-containing complex assembly
Regulatoin of cell morphogenesis
Symbiotic process
Fertilization
Chaperone-mediated protein folding
Toxin transport
0
25
50
75
100
Number of proteins
B
G9a cKO
-log10(p-value)
log2FC
C
G9a-Glp cDKO
ASTL
STAT3
TGON1
HMGB3
CDC25B
DSTN
SET
ROCK1
SKA3
IMPDH2
SIRT1
ERMP1
D
17
(8.3%)
21
(10.3%)
166
(81.4%)
G9a cKO
G9a-Glp cDKO

Figure 4

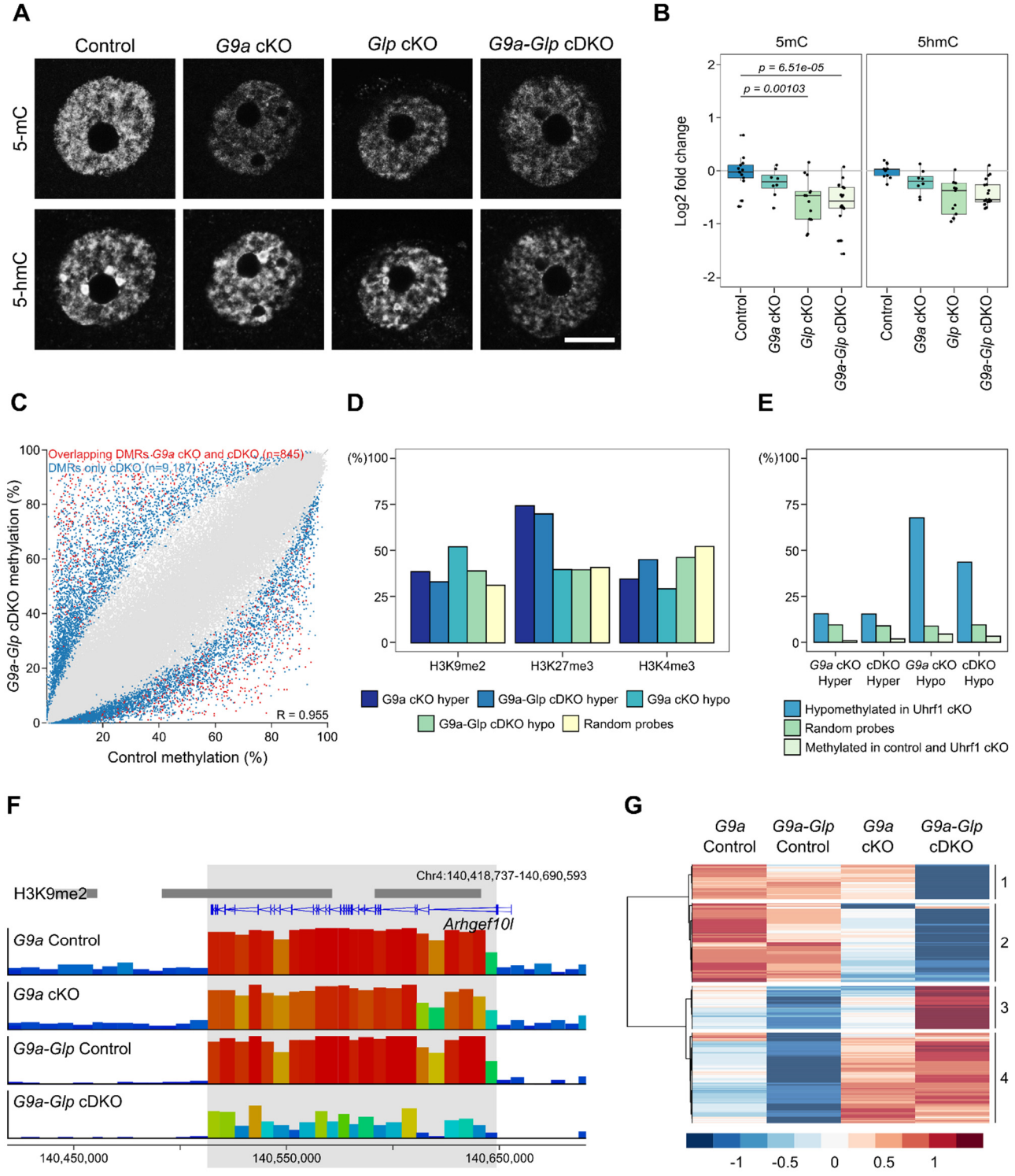
A
Control
G9a cKO
Glp cKO
G9a-Glp cDKO
5-mC
5-hmC
B
5mC
5hmC
p = 6.51e-05
p = 0.00103
Log2 fold change
Control
G9a cKO
Glp cKO
G9a-Glp cDKO
C
Overlapping DMRs G9a cKO and cDKO (n=845)
DMRs only cDKO (n=9,187)
G9a-Glp cDKO methylation (%)
Control methylation (%)
R = 0.955
D
(%)
H3K9me2
H3K27me3
H3K4me3
G9a cKO hyper
G9a-Glp cDKO hyper
G9a cKO hypo
G9a-Glp cDKO hypo
Random probes
E
G9a cKO Hyper
cDKO Hyper
G9a cKO Hypo
cDKO Hypo
Hypomethylated in Uhrf1 cKO
Random probes
Methylated in control and Uhrf1 cKO
F
H3K9me2
Chr4:140,418,737-140,690,593
Arhgef10l
G9a Control
G9a cKO
G9a-Glp Control
G9a-Glp cDKO
140,450,000
140,550,000
140,650,000
G
G9a Control
G9a-Glp Control
G9a cKO
G9a-Glp cDKO
1
2
3
4
-1
-0.5
0
0.5
1

Figure 5

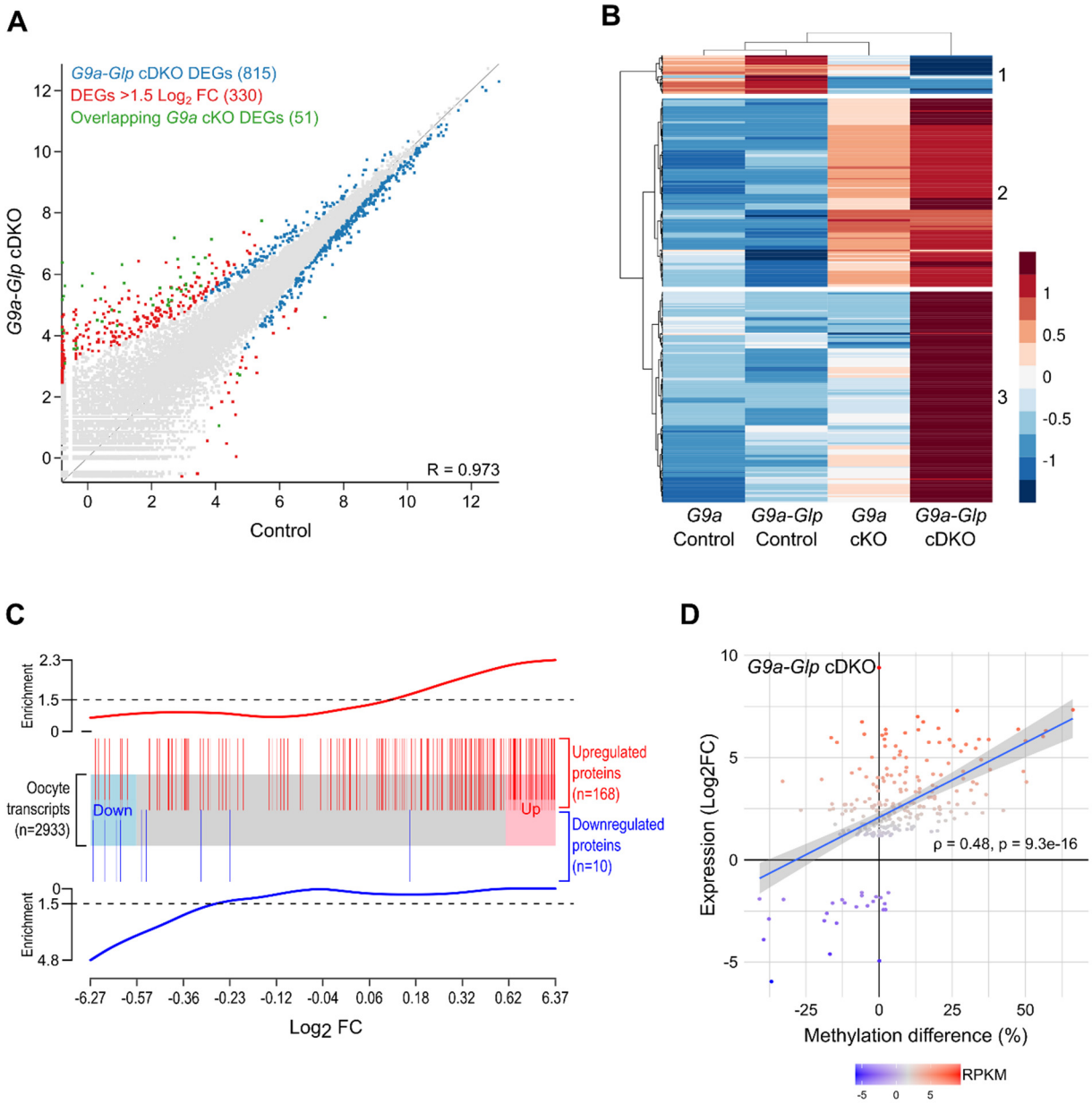
A
G9a-Glp cDKO DEGs (815)
DEGs >1.5 Log2 FC (330)
Overlapping G9a cKO DEGs (51)
G9a-Glp cDKO
Control
R = 0.973
B
1
2
3
G9a Control
G9a-Glp Control
G9a cKO
G9a-Glp cDKO
C
Enrichment
Oocyte transcripts (n=2933)
Down
Up
Upregulated proteins (n=168)
Downregulated proteins (n=10)
Log2 FC
D
G9a-Glp cDKO
Expression (Log2FC)
Methylation difference (%)
ρ = 0.48, p = 9.3e-16
RPKM

Figure 6

Distinct roles for G9A and GLP in the oocyte

Control	*G9a* cKO	*Glp* cKO	*G9a-Glp* cDKO
G9a GLP G9a-Glp heterodimer as predominant form	GLP GLP G9a GLP homodimer	G9a G9a GLP G9a homodimer not stable	G9a GLP No G9a nor GLP
	Reduced littersize	Embryonic lethal	Embryonic lethal
Direct regulation: - H3K9me2 - H3K9me1? - Non-histone targets? Direct or indirect regulation: - Transcription - Protein abundance - DNA methylation - Oocyte maturation - Meiosis	Compensation or direct function of GLP: - H3K9me1 - Proteome - Oocyte maturation Deregulated processes: - H3K9me2 depletion - Small transcriptional changes - Regional changes in DNA methylation - Abnormal meiosis	Deregulated processes: - H3K9me2 depletion and decreased H3K9me1 - Reduced oocyte maturation - Abnormal meiosis Not investigated: - Transcription - Protein abundance - DNA methylation	Deregulated processes: - H3K9me2 depletion and decreased H3K9me1 - More transcriptional changes - More and larger changes in DNA methylation - Changes in protein abundance - Reduced oocyte maturation - Abnormal meiosis

B

H3K9 methylation

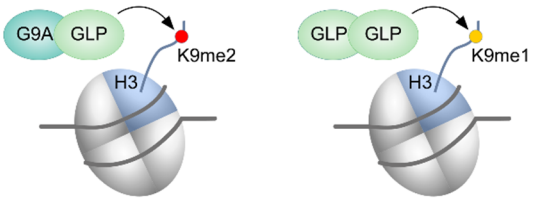

C

UHRF1-dependent hypomethylation

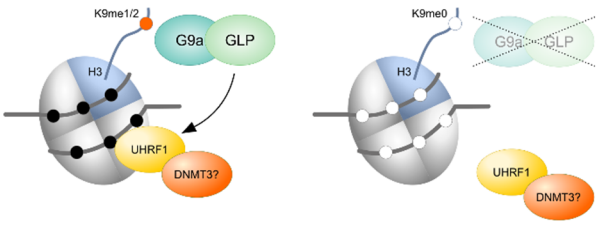

D

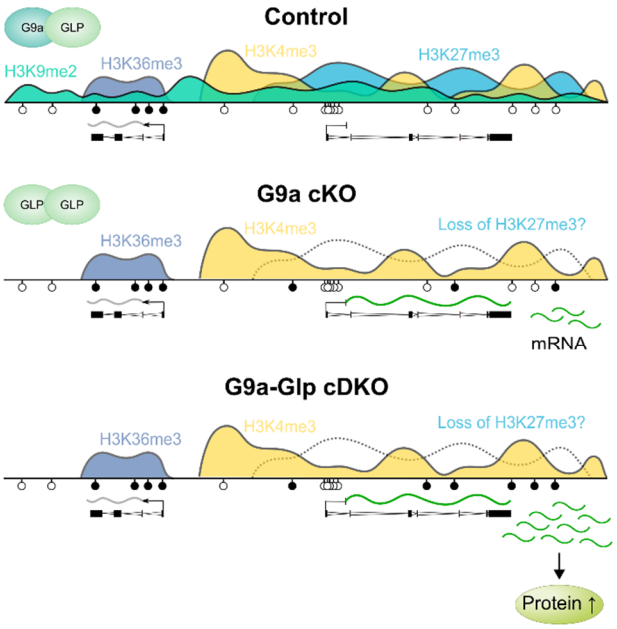

Supplemental Figures

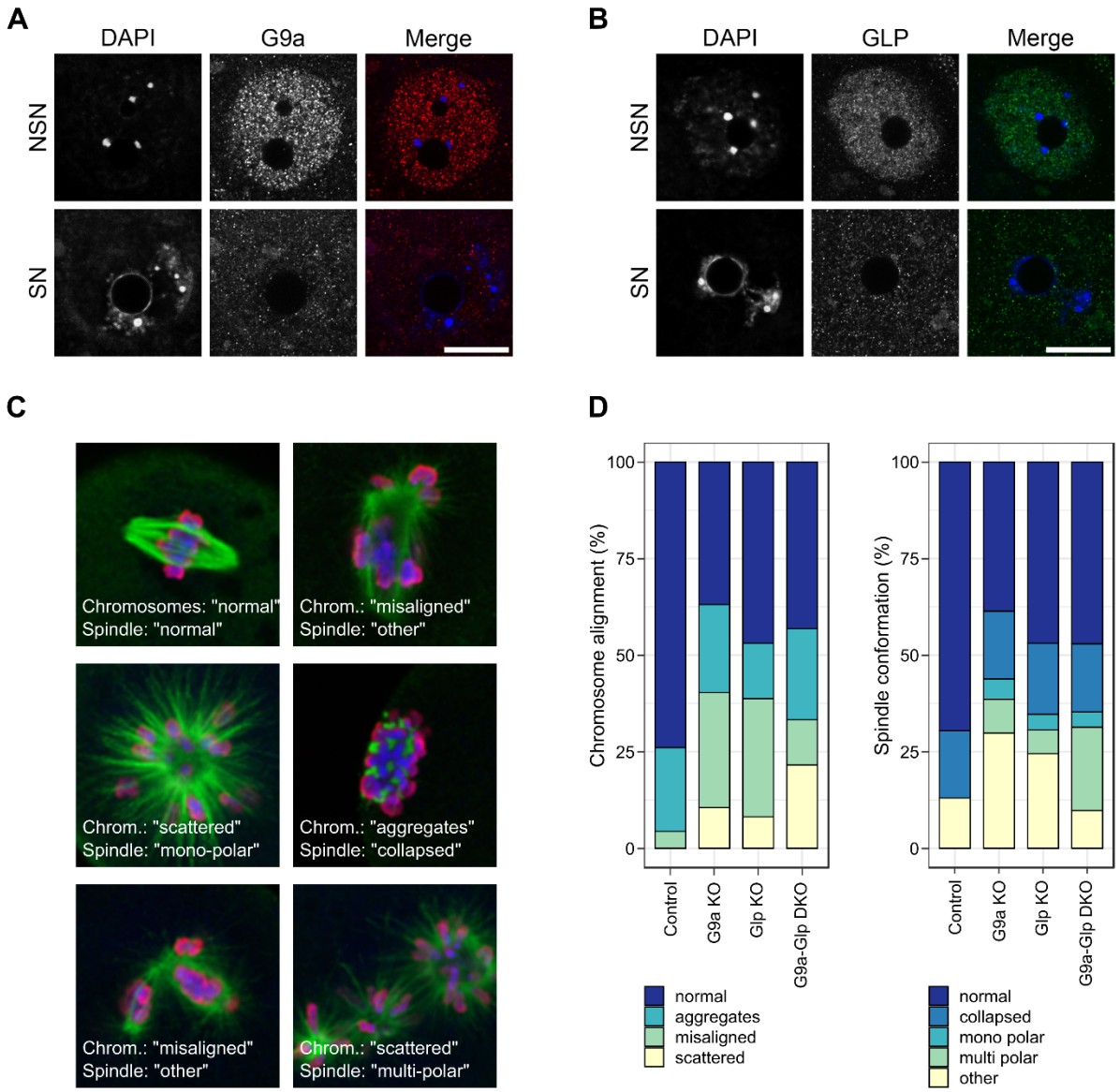

Figure S1: G9A and GLP expression in the oocyte and their effects on meiosis

A, B) Representative images showing DNA stained with DAPI, G9A expression **(A)** and GLP expression **(B)** in NSN and SN control oocytes. The scale bar represents 20µm. **C)** Example images showing meiotic abnormalities observed in MII oocytes. The spindle is stained with an anti-α-tubulin antibody (green) and the chromatin with DAPI (blue) and anti-pan-histone (red). **D)** Stacked bar charts showing the percentage of types of meiotic abnormalities (chromosome alignment and spindle conformation) observed in oocytes.

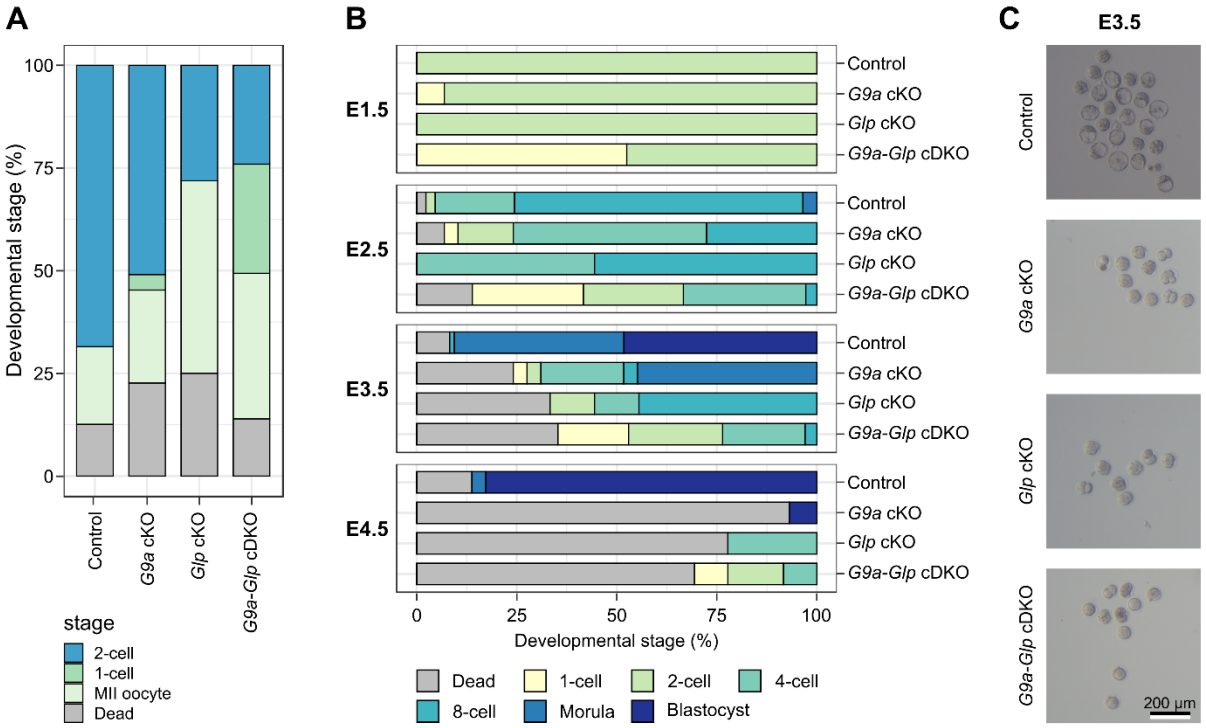

D

Genotype	Normal embryos	Abnormal embryos	Resorption sides	Total embryos
Control	7	1	0	8
G9a cKO	7	2	0	9
G9a cKO	4	4	0	8
Glp cKO	0	3	0	3
G9a-Glp cDKO	0	4	0	4
G9a-Glp cDKO	0	2	0	2

F

Genotype	Normal embryos	Abnormal embryos	Resorption sides	Total embryos
Control	5	1	2	8
Control	8	0	0	8
Control	5	1	2	8
G9a cKO	5	1	3	9
G9a cKO	4	2	2	8
G9a cKO	4	1	2	7
G9a-Glp cDKO	0	0	1	1
G9a-Glp cDKO	0	0	3	3
G9a-Glp cDKO	1	0	1	2

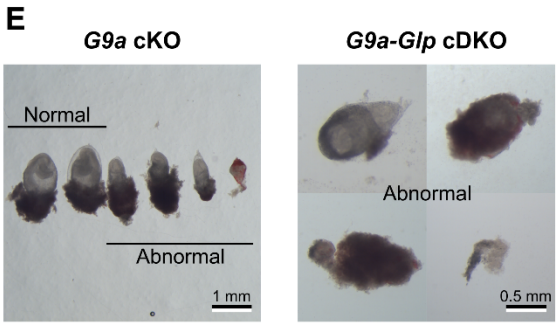

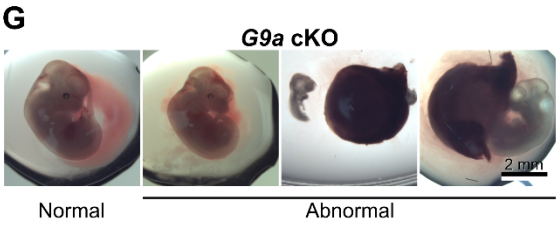

Figure S2: *In vitro* preimplantation and *in vivo* postimplantation development of embryos lacking maternal G9A and/or GLP.

A) Stacked barchart showing developmental stage of embryos collected at E1.5 after superovulation and natural mating with C57Bl6/Babr WT males. One-way ANOVA with Tukey's posthoc test: 2-cell stage Control vs G9a-Glp cDKO P = 0.0068**. **B)** Stacked barcharts showing developmental stage of embryos cultured in vitro after natural mating on E1.5, E2.5, E3.5 and E4.5. One-way ANOVA with Tukey's posthoc test: morula stage Control vs *G9a* cKO *P = 0.0006****. **C)** Images showing examples of embryos cultured in vitro on E3.5. **D, E)** Table showing embryo development at E8.5 **(D)** and E12.5 **(E)** after natural mating of conditional KO females with WT males. Each line represents one female mouse. Indicated are the number of normal embryos, abnormal embryos and resorption sides for each female.

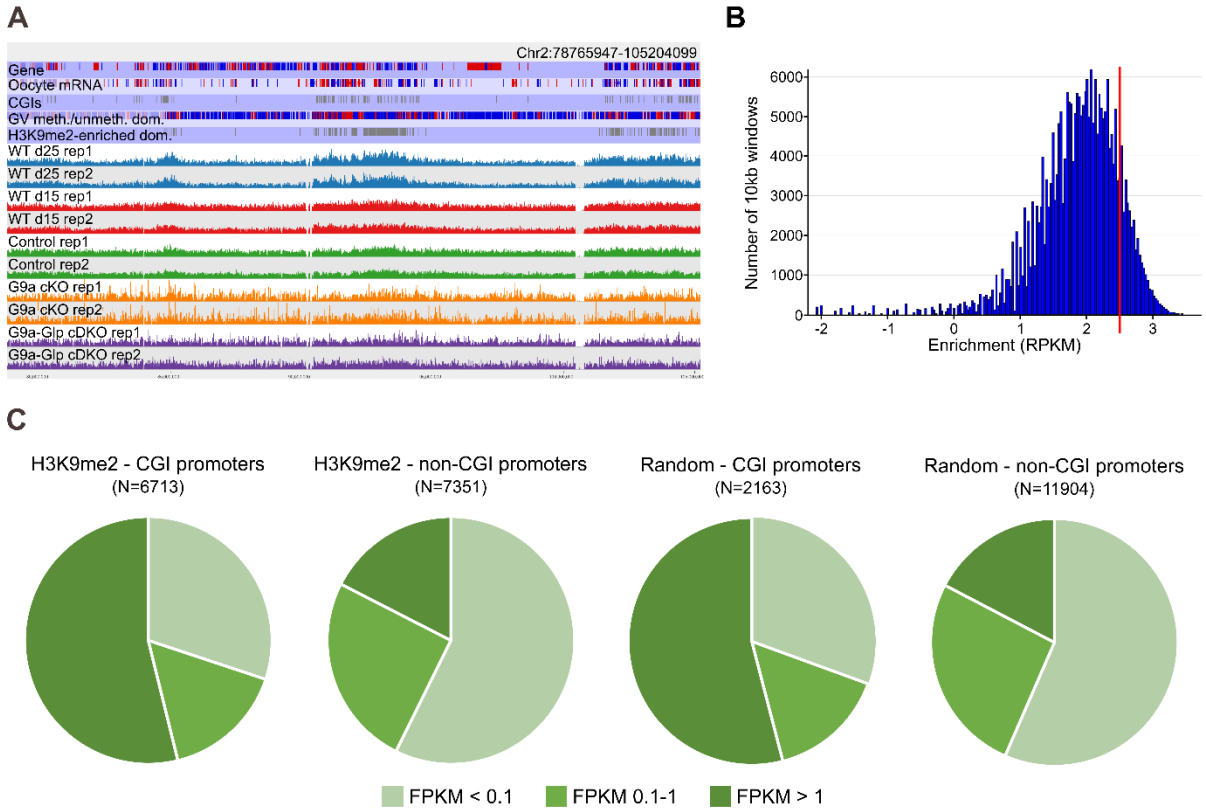

Figure S3: ChIP-seq analysis showing H3K9me2 distribution in control, *G9a* cKO and *G9a-Glp* cDKO oocytes.

A) Screenshot showing H3K9me2 enrichment and reproducibility of replicates. **B)** Histogram showing number of 10 kb windows with a certain enrichment level in d25 WT oocytes. The red line indicates the threshold set to define H3K9me2 enrichment (RPKM > 2.5). **C)** Pie charts showing overlap of H3K9me2 enriched and random probes with untranscribed (FPKM < 0.1), lowly transcribed (FPKM 0.1-1) and highly transcribed genes (FPKM > 1).

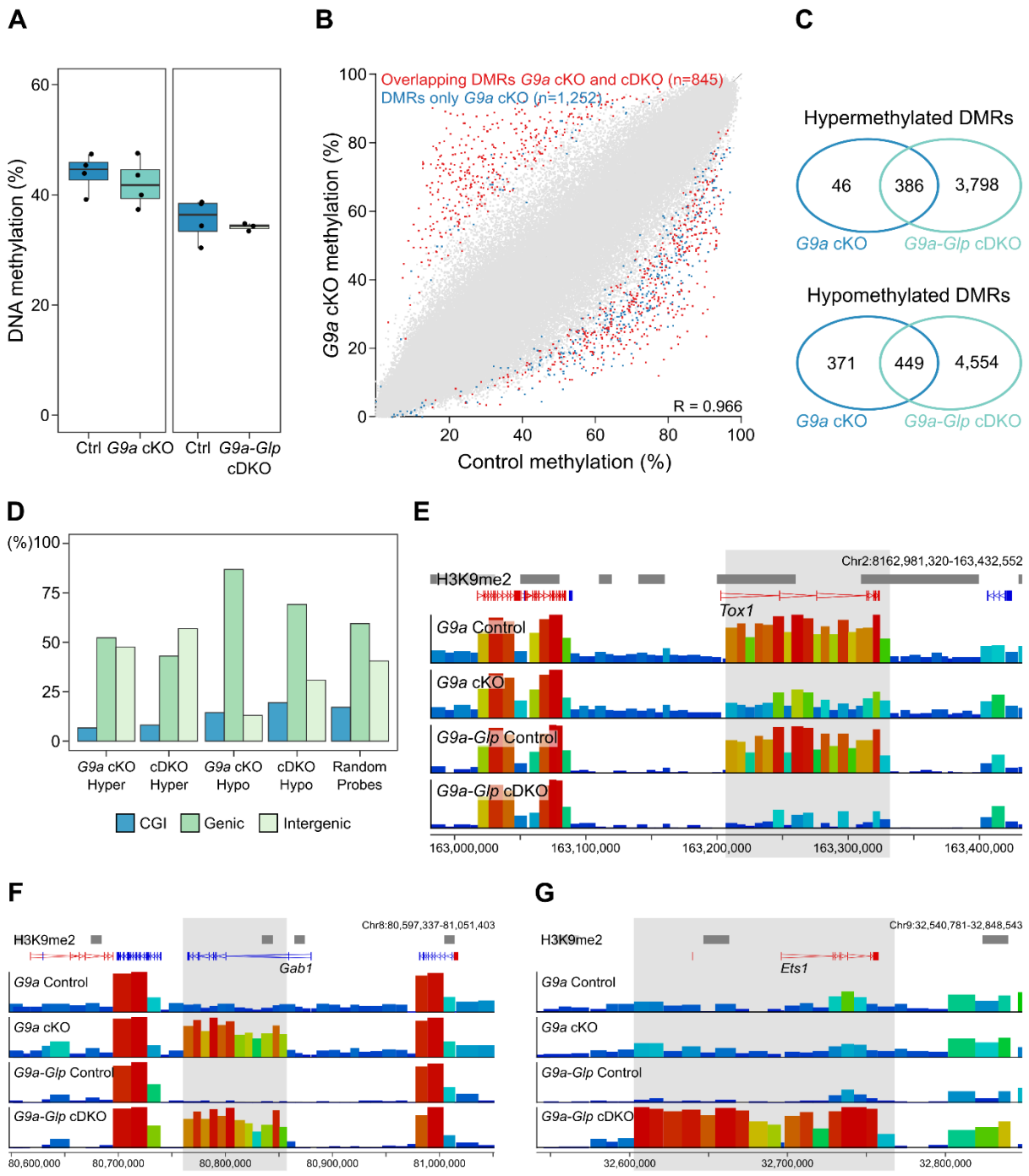

Figure S4: DNA methylation analysis of *G9a* cKO and *G9a-Glp* cDKO oocytes with corresponding littermate controls.

A) Box-whisker plots showing global DNA methylation levels using average methylation levels of 100 CpG windows. Ctrl *vs G9a* cKO *P* = 0.5378; Ctrl vs *G9a-Glp* cDKO *P* = 0.6077 **B)** Scatterplot showing methylation levels of control vs *G9a* cKO oocytes. Unique *G9a* cKO DMRs are highlighted in blue and DMRs shared with *G9a-Glp* cDKO oocytes in red. **C)** Venn diagrams, showing overlap of hypermethylated and hypomethylated DMRs between *G9a* cKO and *G9a-Glp* cDKO oocytes. **D)** Barchart showing percentage of DMRs and random probes overlapping CGIs, genic and intergenic regions. Qi-square comparing genic and intergenic DMRs: G9a cKO *adj. P = 0.026**; all others *P < 0.0001****. **E-G)** Genome screenshots showing examples differentially methylated domains. Shown are a region that is hypomethylated in both *G9a* cKO and *G9a-Glp* cDKO oocytes **(E)**, a region that is hypermethylated in both *G9a* cKO and *G9a-Glp* cDKO oocytes **(F)** and a region that is uniquely hypermethylated in *G9a-Glp* cDKO oocytes **(G)**.

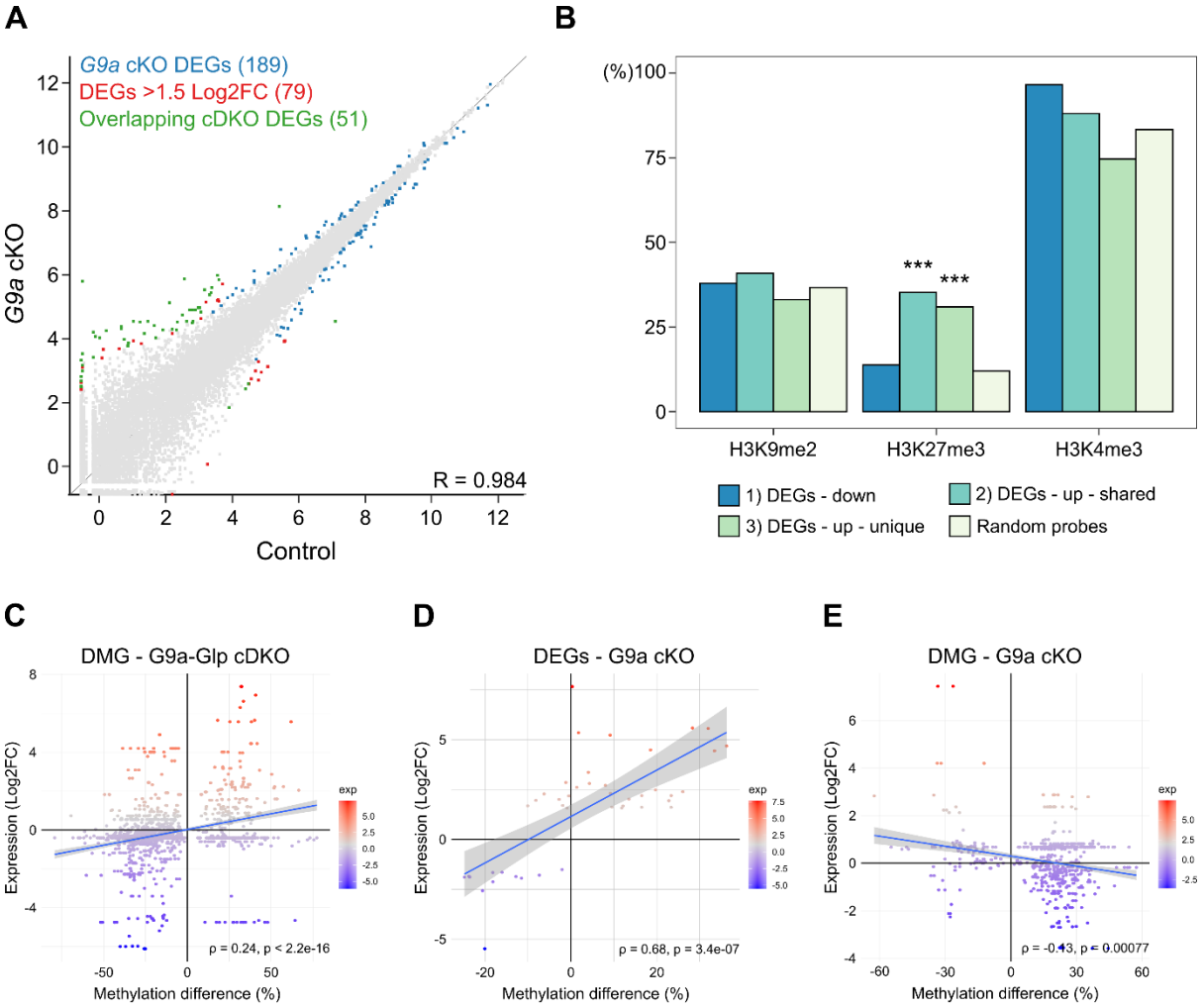

Figure S5: RNA-seq analysis showing transcriptome changes in G9a cKO and G9a cDKO oocytes and their link with DNA methylation.

A) Scatterplot showing expression levels of control vs. *G9a* cKO oocytes. Unique *G9a* cKO DEGs are highlighted in blue, DEGs with Log2FC>1.5 in red and DEGs shared with *G9a-Glp* cDKO oocytes in green. **B)** Barchart showing proportion of DEGs overlapping with histone modifications. DEGs are split according to the clustering analysis of **Figure 5B**. Qi-square analysis comparing DEGs to random probes: *P < 0.0001****. **C)** Plot showing link between methylation and expression changes of differentially methylated genes in G9a-Glp cDKO oocytes. **D, E)** Plot showing link between methylation and expression changes of differentially expressed genes (C) and differentially methylated genes (D) in G9a cKO oocytes. **C-E)** Expression levels are indicated by the colour scale. Spearman correlation indicated in plot.